DOI: 10.1534/genetics.108.092775

Coprinus cinereus rad50 Mutants Reveal an Essential Structural Role for Rad50 in Axial Element and Synaptonemal Complex Formation, Homolog Pairing and Meiotic Recombination

Sonia N. Acharya,*[,1] Alexander M. Many,*[1,2] Andrew P. Schroeder,* Felicia M. Kennedy,* Oleksandr P. Savytskyy,* Jennifer T. Grubb,* Jack A. Vincent,* Elizabeth A. Friedle,* Martina Celerin,* Daniel S. Maillet,* Heather J. Palmerini,* Megan A. Greischar,* Gabriel Moncalian,[†,3] R. Scott Williams,[†] John A. Tainer[†] and Miriam E. Zolan*[,4]

**Department of Biology, Indiana University, Bloomington, Indiana 47405 and* [†]*The Scripps Research Institute, La Jolla, California 92037*

Manuscript received June 17, 2008
Accepted for publication October 17, 2008

ABSTRACT

The Mre11/Rad50/Nbs1 (MRN) complex is required for eukaryotic DNA double-strand break (DSB) repair and meiotic recombination. We cloned the *Coprinus cinereus rad50* gene and showed that it corresponds to the complementation group previously named *rad12*, identified mutations in 15 *rad50* alleles, and mapped two of the mutations onto molecular models of Rad50 structure. We found that *C. cinereus rad50* and *mre11* mutants arrest in meiosis and that this arrest is Spo11 dependent. In addition, some *rad50* alleles form inducible, Spo11-dependent Rad51 foci and therefore must be forming meiotic DSBs. Thus, we think it likely that arrest in both *mre11-1* and the collection of *rad50* mutants is the result of unrepaired or improperly processed DSBs in the genome and that Rad50 and Mre11 are dispensable in *C. cinereus* for DSB formation, but required for appropriate DSB processing. We found that the ability of *rad50* mutant strains to form Rad51 foci correlates with their ability to promote synaptonemal complex formation and with levels of stable meiotic pairing and that partial pairing, recombination initiation, and synapsis occur in the absence of wild-type Rad50 catalytic domains. Examination of single- and double-mutant strains showed that a *spo11* mutation that prevents DSB formation enhances axial element (AE) formation for *rad50-4*, an allele predicted to encode a protein with intact hook region and hook-proximal coiled coils, but not for *rad50-1*, an allele predicted to encode a severely truncated protein, or for *rad50-5*, which encodes a protein whose hook-proximal coiled-coil region is disrupted. Therefore, Rad50 has an essential structural role in the formation of AEs, separate from the DSB-processing activity of the MRN complex.

MEIOSIS is the unique type of cell division that results in the production of haploid gametes. During prophase I, homologs condense, pair, and recombine. At least one recombination event per homologous pair becomes a crossover, which, in combination with sister-chromatid cohesion, creates a chiasma that holds homologs together as they attach to the metaphase I spindle. Release of sister-chromatid cohesion along chromosome arms allows anaphase I separation of homologs, and release of centromere cohesion allows anaphase II separation of sister chromatids.

Meiotic recombination events initiate with a Spo11-catalized DNA double-strand break (DSB), and some of the proteins required for meiotic recombination have been recruited from mitotic DNA repair pathways. A primary example is the complex of proteins referred to as Mre11, Rad50, and Nbs1 (MRN). Evidence from *Saccharomyces cerevisiae*, in which the Nbs1 ortholog is called Xrs2, showed that the MRN complex is necessary for meiotic DSB formation by Spo11 (Alani *et al.* 1990; reviewed in Borde 2007). However, in other species different results have been obtained. In *Caenorhabditis elegans*, Rad50 facilitates DSB formation by Spo11 but is apparently not strictly required for Spo11 activity (Hayashi *et al.* 2007). In *Schizosaccharomyces pombe* (Young *et al.* 2004), *Arabidopsis thaliana* (Puizina *et al.* 2004), and *Drosophila melanogaster* (Mehrotra and McKim 2006) the MRN complex is required for break processing but not break formation.

In all eukaryotic organisms studied, *mre11*, *rad50*, and *xrs2/nbs1* mutants exhibit meiotic recombination defects and radiation sensitivity (Cox and Parry 1968;

Sequence data from this article have been deposited with the EMBL/GenBank Data Libraries under accession no. 1017584.

[1]These authors contributed equally to this work.

[2]*Present address:* Department of Oncological Sciences, Mount Sinai School of Medicine, New York, NY 10029.

[3]*Present address:* Instituto de Biomedicina y Biotecnología de Cantabria, 39011 Santander, Spain.

[4]*Corresponding author:* Department of Biology, Indiana University, 1001 E. Third St., Bloomington, IN 47405. E-mail: mzolan@indiana.edu

Game *et al.* 1980; Malone and Esposito 1981; Malone 1983; Alani *et al.* 1990; Ivanov *et al.* 1992; Ajimura *et al.* 1993; Ramesh and Zolan 1995; Tavassoli *et al.* 1995; Carney *et al.* 1998; Chamankhah *et al.* 1998; Matsuura *et al.* 1998; Varon *et al.* 1998; Stewart *et al.* 1999; Gerecke and Zolan 2000; Gallego *et al.* 2001; Hartsuiker *et al.* 2001; Pitts *et al.* 2001; Hayashi *et al.* 2007). The members of the Mre11 complex have been grouped by epistasis analysis (Game *et al.* 1980; Malone and Esposito 1981; Ivanov *et al.* 1992; Ajimura *et al.* 1993; Valentine *et al.* 1995) and have been shown to directly interact (Johzuka and Ogawa 1995; Petrini *et al.* 1995; Dolganov *et al.* 1996; Trujillo *et al.* 1998; Varon *et al.* 1998). Mammalian deletion mutants of the Mre11 complex exhibit embryonic lethality (Xiao and Weaver 1997; Luo *et al.* 1999; Yamaguchi-Iwai *et al.* 1999; Zhu *et al.* 2001). Viable mutations in human homologs of the MRN complex invariably result in syndromes characterized by a loss of fertility, and cancer early in life (Carney *et al.* 1998; Matsuura *et al.* 1998; Varon *et al.* 1998; Stewart *et al.* 1999; Pitts *et al.* 2001; Bender *et al.* 2002). The biochemical properties of the individual proteins composing this complex have been characterized in mammals and yeast (reviewed in Williams *et al.* 2007). Mre11 binds DNA and exhibits *in vitro* ssDNA endonuclease and Mn^{2+}-dependent 3′–5′ double-stranded DNA exonuclease activities (Paull and Gellert 1998). Both Mre11 nuclease activity and homodimerization are important for DSB repair (Williams *et al.* 2008). Rad50 is an ATP-dependent DNA binding protein that forms a multimer (Raymond and Kleckner 1993; Hopfner *et al.* 2000a) and has both ATPase and adenylate kinase activities that are important for protein function (Bhaskara *et al.* 2007). Rad50 is furthermore a prototype for a superfamily of SMC proteins and ABC transporters (Hopfner and Tainer 2003). The Nbs1 protein serves to localize the complex in the nucleus (Tauchi *et al.* 2001), modifies MRN complex activity (Paull and Gellert 1999), and plays a primary role in signal transduction after DNA damage (Lee and Paull 2004, 2005).

Partial *Pyrococcus furiosus* Rad50/Mre11 complexes have been crystallized by Hopfner *et al.* (2000b, 2001). Rad50 has two α-helical coiled-coil domains separated by a flexible hinge (referred to as a hook) harboring a semi-zinc finger at the center. The N and C termini of the protein are globular in nature and together compose a functional ATP-binding site. They are brought into contact with each other by an intertwining of the N- and C-terminal coils. The two interwoven coils form a flexible rod, creating a binding site for Mre11 made up of acidic residues just adjacent to the globular domain (Hopfner *et al.* 2001). Crystallographic and biochemical data (Hopfner *et al.* 2002a) have confirmed a role in protein dimerization for the conserved semi-zinc finger in the hook region (Sharples and Leach 1995). Current models (Hopfner *et al.* 2002a,b; Williams and Tainer 2005) suggest that hook interactions of Rad50 molecules allow bridging of either sister chromatids or DSB ends. These Rad50 molecules are also held together with the aid of two dimerized Mre11 molecules at each opposing head of the complex (Williams *et al.* 2008). Recent atomic force microscopy studies (Moreno-Herrero *et al.* 2005) showed that MRN complexes change conformation upon DNA binding. The unbound complexes exhibit greater flexibility of the coiled-coil regions, which may favor intracomplex interactions, whereas the coiled coils of DNA-bound complexes are more rigid and parallel, thus favoring intercomplex interactions that would facilitate complex ability to bridge and stabilize DNA ends (Williams and Tainer 2005).

Meiotic defects in *rad50* mutants (reviewed in Borde 2007; Cherry *et al.* 2007) include failure of Spo11-dependent DSB formation or processing (Alani *et al.* 1990; Young *et al.* 2004; Mehrotra and McKim 2006; Hayashi *et al.* 2007), incomplete formation of axial elements (AE) and the synaptonemal complex (SC) (Alani *et al.* 1990), and the formation of nonviable products (Alani *et al.* 1990; Young *et al.* 2004). Thus, it has a central role in meiotic recombination and chromosome metabolism.

We cloned the *rad50* gene and examined members of the MRN complex in the basidiomycete *Coprinus cinereus*. *C. cinereus* has naturally synchronous meiosis (Raju and Lu 1970), well-developed cytogenetics (Pukkila *et al.* 1984; Pukkila and Lu 1985; Seitz *et al.* 1996; Li *et al.* 1999), and an annotated genomic sequence (Stajich *et al.* 2006). In screens for mutants defective in both the survival of gamma radiation and meiosis (Zolan *et al.* 1988; Valentine *et al.* 1995), we identified four complementation groups, termed *rad3*, *rad9*, *rad11*, and *rad12*. These four genes are all part of the same gamma radiation survival pathway (Valentine *et al.* 1995; Cummings *et al.* 2002). The gene *rad11* was cloned and found to encode the *C. cinereus* ortholog of Mre11 (Gerecke and Zolan 2000). Therefore, we reasoned that one of the other genes of the group would encode the *C. cinereus* ortholog of Rad50. Here we present our finding that the *C. cinereus* gene initially named *rad12* (Ramesh and Zolan 1995) encodes Rad50 and examine critical features of the role of Rad50 in meiosis.

MATERIALS AND METHODS

Strains and culture conditions: The wild-type dikaryon used for the Rad51 time-course experiment shown in Figure 4 has been previously described (Valentine *et al.* 1995). *rad50* mutant strains were generated in five separate mutant screens (Zolan *et al.* 1993, 1995; Ramesh and Zolan 1995; Valentine *et al.* 1995), all starting with the strain Java-6 (Binninger *et al.* 1987). Strain Okayama-7 (Wu *et al.* 1983) was used for all outcrosses and backcrosses. Of the *rad50* strains examined in this study, *rad50-1*, *rad50-2*, *rad50-3*, *rad50-4*, *rad50-5*, *rad50-6*,

rad50-8, *rad50-14*, and *rad50-15* were outcrossed and then backcrossed four times; *rad50-10*, *rad50-11*, and *rad50-16* were outcrossed and then backcrossed once; and *rad50-7*, *rad50-9*, *rad50-12*, and *rad50-13* were outcrossed only.

The *rad50-1;spo11-1*, *rad50-4;spo11-1*, *rad50-5;spo11-1*, *rad50-8;spo11-1*, and *mre11-1;spo11-1* strains were generated by crossing a *rad50* or a *mre11* single mutant to *R126-49* [*spo11-1* (A_mB_m); Cummings *et al.* 1999; Celerin *et al.* 2000]. Double mutants were identified by subjecting progeny to a radiation-sensitivity chunk test (Zolan *et al.* 1988) to test for the *rad50* or the *mre11* mutation. All strains except those used to construct the *mre11-1;spo11-1* double mutant were then mated to *spo11-1* strains with $A_{42}B_{42}$ or $A_{43}B_{43}$ mating types. Strains that mated to *spo11-1;*$A_{43}B_{43}$ only, fruited white (sporeless), and were radiation sensitive were scored as $A_{42}B_{42}$ double mutants. These in turn were mated to strain Okayama-7 ($A_{43}B_{43}$) to generate double mutants, sibling single mutants, and wild-type controls with both $A_{42}B_{42}$ and $A_{43}B_{43}$ mating types. Compatible monokaryons were mated and used for further analysis. For construction of the *mre11-1;spo11-1* double mutant, progeny were screened for hygromycin resistance as a marker for the insertional mutation in *spo11-1* (Celerin *et al.* 2000). Strain genotype was confirmed by sequencing and/or diagnostic restriction digests of PCR-amplified fragments containing the mutated region. Mating pairs were identified as previously described (Zolan *et al.* 1988).

Spore viability: Spore viabilities were determined using the spotted drop method described in Celerin *et al.* (2000). Spores were serially diluted and 10-μl drops were spotted onto a gridded plate. Five to seven mushroom caps were counted per strain and analyzed using the ANOVA test (SPSS 10.0 for the Macintosh).

Degenerate PCR amplification of *Ccrad50*: Rad50 homologs from other organisms were aligned using ClustalX (Thompson *et al.* 1997). Regions of high conservation were used as the basis for the design of degenerate primers. *rad50* was amplified from *C. cinereus* genomic DNA using a degenerate primer pair: F1, 5′ AAR ACN ACN ATH ATH GAR TGY YTN 3′, and R1, 5′ GGG NWS RTC YTC YTG RTG RCA RAA D 3′, corresponding to amino acids 38–46 and 158–165 of CcRad50. A product corresponding to *rad50* was used to probe a chromosome 8- and 9-enriched cosmid library of strain Okayama-7 (Zolan *et al.* 1992). Three cosmids were isolated: 3B6, 5F8, and 23G1. The cosmid 23G1 was found to contain a complete copy of *rad50* through subsequent sequencing analysis.

RFLP analysis: Strain Okayama-7 and a fourth-generation backcrossed *rad12-4* strain (*rad12-4;4-1*) were mated. Progeny were analyzed as described in Gerecke and Zolan (2000) except that all genomic DNA was digested with *Eco*RI and probed with a 3B6 cosmid containing *Ccrad50*.

Transformation rescue assay: Transformation rescue of oidial protoplasts of the *C. cinereus rad50-4* mutant was performed as described (Binninger *et al.* 1987; Zolan *et al.* 1992). A *rad50-4;trp1-1,1-6;ade8* strain was transformed with 5 μg of cosmid 23G1. This cosmid also contains the *trp1* gene, and tryptophan prototrophs were selected and assayed as described in Gerecke and Zolan (2000) except that the rescue of meiotic defects was assayed through a mating with a compatible *rad50-4* strain (*rad50-4;4-2*).

Sequencing of wild-type *rad50*: Plasmids containing subclones of genomic DNA of *rad50* were isolated from *Escherichia coli* and initially sequenced with M13F/R or T3/T7 vector primers. Primers for a sequencing walk were based upon the previous sequence data and designed using the OLIGO 5.0 program. Primers for internal sequencing and amplification were made by Genosys or by MWG-Biotech. PCR products were sequenced using standard techniques. Sequences were edited and made contiguous by Sequencher v.3.1.1 (Gene Codes), and translated by DNASIS v.2.0 (Hitachi Software Engineering). Predicted proteins were identified using the blastx program in BLAST (Altschul *et al.* 1990) and alignments were performed using Clustal X (Thompson *et al.* 1997). Coiled structure of Rad50 was predicted using the MultiCoils program (Wolf *et al.* 1997).

Sequencing of *rad50* cDNA: First-strand cDNA synthesis using reverse transcriptase (SuperScript II; GibCo-BRL Life Technologies, Gaithersburg, MD) was performed on poly(A)$^+$ mRNA isolated from mushroom caps at 1 hr after karyogamy (K + 1). A gene-specific amplification was then performed using a *rad50* primer pair. The product was run on an agarose gel and Southern blotted. It was then probed with an amplified piece of *rad50*. A band that hybridized to *rad50* DNA was gel extracted and cloned into a TOPO-TA vector. The resulting clones were sequenced using vector primers and shown to correspond to a 1.1-kb fragment of 3′ *rad50* cDNA. A reverse primer was made, extending across 10 bp of exon sequence immediately following the 3′ and 5′ flank of intron 17. In this way we eliminated amplification of genomic sequence. This primer was used to extend the oligo (dT) first-strand cDNA synthesis reaction farther. This first-strand synthesis reaction was used as a template for an amplification with a forward primer across intron 15. This fragment was sequenced. A new first-strand cDNA synthesis reaction was then performed, using a reverse primer across intron 15 and poly(A)$^+$ mRNA isolated from mushroom caps at K + 6. This first-strand reaction was amplified (Advantage 2.0 kit, BD Biosciences–Clontech) with a forward primer from the beginning of the *rad50* genomic sequence. This product was also sequenced. Several primers in the 5′-UTR were used to amplify the 5′ end of *rad50* with a reverse primer that spanned the fourth intron. These products were sequenced. Sequences were made contiguous using the Sequencher program v.3.1.1 (Gene Codes).

Sequencing of mutant *rad50* alleles: Primers for internal sequencing and amplification were based upon the wild-type sequence data and designed using the OLIGO 5.0 program. Overlapping regions of DNA for sequencing original *rad50* mutant strains were amplified by PCR and directly sequenced. Template DNA for amplification reactions consisted of *rad50* mutant genomic DNA extracted from vegetative tissue (Zolan and Pukkila 1986). PCR products were desalted using the QIAquick PCR purification kit or extracted from agarose gels using the QIAEX II kit (QIAGEN, Valencia, CA). Sequencing and analysis were performed using standard procedures.

RT–PCR on *Ccrad50* mutants: RT–PCR was performed on RNA extracted from heterozygotes of *rad50* mutant and wild-type mushrooms. The two strains, *rad50-1* and *rad50-4*, were mated to strain PJP 307, a meiotically wild-type strain. The resulting dikaryons were subcultured twice and poly(A)$^+$ RNA was extracted from meiotic tissue at K + 6 (RNeasy plant mini kit, QIAGEN; PolyATtract System 1000, Promega, Madison, WI). First-strand cDNA was made using the Superscript kit (GibCo-BRL Life Technologies). For *rad50-1*, primers were designed to be cDNA specific and to span introns 3 and 5. For *rad50-4*, a cDNA-specific forward primer spanning intron 19 was used in combination with a 3′-UTR reverse primer or an intron 22-spanning cDNA-specific primer. PCR amplification and sequencing were performed by standard techniques.

Protein modeling of *CcRad50* mutants: Protein models were based on the structures of the *P. furiosus* Rad50 protein (RCSB codes 1F2U and 1L8D) (Hopfner *et al.* 2000b, 2002a). CcRad50, CcRad50-4, and CcRad50-5 models were created with MOLSCRIPT (Kraulis 1991) and PYMOL (http://www.pymol.org).

Electron microscopy: Chromosome spreads were performed as described by Pukkila *et al.* (Pukkila and Lu 1985; Pukkila *et al.* 1992). Silver nitrate staining of meiotic nuclei

was performed as per Seitz *et al.* (1996). Grids were prepared as per Pukkila *et al.* (1992) and viewed with a JEOL-1010 electron microscope. Images of stained nuclei were scanned into a computer and analyzed using Adobe Photoshop 7.0 (Adobe Systems), National Institutes of Health (NIH) Image 1.63 (Wayne Rasband, NIH), and Microsoft Excel '98.

Epistasis analysis of late meiotic phenotypes: Slices of cap tissue were taken at various time points after karyogamy (as defined in Seitz *et al.* 1996), and veil cells were peeled and discarded. The tissue was stored in 70% ethanol, 30% NS buffer (20 mm Tris–HCl, pH 7.5, 0.25 m mannitol, 1 mm EDTA, 1 mm $MgCl_2$, 0.1 mm $CaCl_2$) at 4°. Single gill layers of meiotic cells were dissected and mounted onto ProbeOn Plus (Fisher Scientific, Pittsburgh) microscope slides with 4′,6-diamidino-2-phenylindole dihydrochloride (DAPI; Vectashield, Vector Laboratories, Burlingame, CA) and examined. For the *rad50* experiments (Figure 3, A–C), slides were examined using a Nikon Microphot-FXA microscope with a Ludl filterwheel. Images of stained nuclei were captured using a Photometrics cooled digital CCD camera system and Quips XL SmartCapture/IP Lab Spectrum imaging software (Vysis). For the *mre11-1* experiments (Figure 3D), images were taken using a Nikon E800 fluorescence microscope, driven by the Metamorph imaging system (Molecular Devices). Images were taken as *z*-series stacks using a step size of 0.09 μm, capturing all planes in which the tissue sample was in focus. Each stack was then flattened into a single image, using the maximum pixel brightness.

Rad51 protein expression and purification: We constructed a Rad51 protein expression construct by cloning the full-length *rad51* cDNA (Stassen *et al.* 1997) into the pET-30 expression vector (Novagen), which was then transformed into BL21(DE3) cells for expression. Protein expression conditions are similar to Novagen company literature and alterations are described in full in supplemental methods.

Anti-Rad51 antibody production: Purified Rad51 in SDS–PAGE gel slices was sent to Cocalico Biologicals (Reamstown, PA) and used for immunization of rabbits according to their injection schedule, using the acrylamide as the adjuvant.

Affinity purification of anti-Rad51 antibody: To remove vector-encoded tags, serum was adsorbed using an affinity column made with a portion of Mre11 expressed in the same vector. Anti-Rad51 antibody was then purified using a second affinity column. A detailed description is in supplemental methods.

Commercial antibodies: Anti-human Rad51 was obtained from Calbiochem (San Diego; La Jolla, CA) (PC130). Purified nonspecific IgG from rabbit serum was obtained from Sigma (St. Louis) (18140).

Immunostaining of chromosome spreads: Staining of chromosome spreads was performed using the following protocol, which was adapted from Sym *et al.* (1993). Chromosome spreads were obtained as described (Pukkila *et al.* 1992; Seitz *et al.* 1996) except that we used uncharged slides (VWR), cleaned with Sparkle glass cleaner (A. J. Funk and Co.). Slides with chromosome spreads were wetted in PBS, pH 7.4, for 10 min. The slides were then blocked with 100 μl of PBS containing 5% BSA and 1% normal goat serum (Vector Laboratories catalog no. S-1000) twice for 15 min each at room temperature, under a parafilm coverslip. The slides were incubated with 100 μl anti-Rad51 antibody diluted to a final concentration of 1 μg/ml in PBS containing 5% BSA, covered with a parafilm coverslip, and incubated overnight protected from light in a humid environment. Slides were then washed three times for 10 min each with PBS + 0.05% Tween-20 at room temperature. Secondary antibody was then added to the slides at a final concentration of 1.2 μg/ml, in 5% BSA dissolved in PBS, for 4 hr at room temperature, protected from light in a humid environment. Slides were then washed three times for 10 min each with PBS + 0.05% Tween-20 at room temperature. Slides were mounted with DAPI in Vectashield mounting medium, sealed with nail polish, and stored at 4° protected from light until examined. For data analysis, an experiment was defined as the images taken from one slide, made using cells from one mushroom. Slides made from mushrooms that failed to complete fruiting body development were not used. For each combination of strain and time point examined, sufficient experiments were performed that at least two mushrooms were used and the total number of images combined across experiments was ≥30. Antibodies from separate purifications gave statistically similar results; therefore, data obtained using antibodies from different purifications were pooled. For averages and statistical tests, the number of foci from images generated from different experiments was pooled.

Immunostaining of tissue: Meiotic spindles were detected in single layers of meiotic tissue with DM1A mouse anti-α-tubulin antibody (Accurate Chemical and Scientific), using the conditions described in Celerin *et al.* (2000).

Irradiation of *spo11-1*: At K + 1 or K + 3 *spo11-1* mushrooms were irradiated with 60 krad of gamma radiation, using a ^{137}Cs irradiator (Mark 1 model 68-A, J. L. Shepard and Associates), at 1.2 krad/min. Chromosome spreads were made at K + 2 or K + 4, *i.e.*, 10 min after samples were removed from the irradiator.

Fluorescence *in situ* hybridization: Fluorescence *in situ* hybridization (FISH) was performed as described (Li *et al.* 1999). Probes 3 and 6 described in Li *et al.* (1999) were used, representing telomeric and interstitial sites, respectively, of chromosome 13.

Statistical analyses: For spore viability comparisons and for data from immunostraining of chromosome spreads using anti-Rad51 antibody, comparisons between mean numbers for two groups were performed using Student's *t*-test, while multiple pairwise comparisons were performed using an ANOVA test and, where appropriate, Tukey's *post hoc* test. All tests were performed using Minitab or SPSS.

For FISH and electron microscopy (EM) data, statistical comparisons between strains were performed using chi-square tests, using the Excel program (Microsoft). For the analysis of EM data, the categories AE only and SC were pooled.

RESULTS

Cloning of *C. cinereus rad50* and its identification as *rad12*: We aligned Rad50 protein sequences from humans, mice, *S. cerevisiae*, and *A. thaliana* and designed primers to amplify a fragment within the relatively conserved 5′ region of the gene. Using *C. cinereus* genomic DNA as a template, we amplified and sequenced a 363-bp fragment, which BLAST (Altschul *et al.* 1997) analysis showed was likely orthologous to Rad50. Previous restriction fragment length polymorphism (RFLP) mapping had shown that the *C. cinereus rad12* locus is on chromosome 8 in strain Okayama-7 (Zolan *et al.* 1993). Therefore, the *rad50* PCR fragment was used to probe colony blots of a cosmid library enriched for chromosomes 8 and 9 from the Okayama-7 strain of *C. cinereus* (Zolan *et al.* 1992). Three cosmids were isolated, and the *Ccrad50* gene was sequenced from subclones of these cosmids. Because Rad50 orthologs are strongly conserved at the N and C termini, start and stop sites were defined by alignment to other Rad50 proteins. The *C. cinereus* genomic *rad50* gene from strain

Okayama-7 is 5091 bp in length, and the sequence we determined exactly matches the sequence reported for the same strain by the Broad Institute [*Coprinus cinereus* Sequencing Project, Broad Institute of MIT and Harvard (http://www.broad.mit.edu/annotation/genome/coprinus_cinereus/Home.html)].

To determine *rad50* gene structure, we used RT–PCR to isolate overlapping portions of *rad50* cDNA, and we compared cDNA sequence with genomic sequence to identify introns. The *Ccrad50* coding region is 3930 bp in length and is interrupted in the genome by 22 introns (Figure 1A; Table 1; GenBank accession no. 1017584). The predicted protein is 1309 amino acids in length, with a molecular weight of 150.7 kDa (Figure 1B).

To test whether the *rad50* gene maps to the *rad12* genetic locus, we analyzed progeny of a cross between a *rad12-4* strain (*rad12-4;4-1*) and the backcross parent (Okayama-7; Valentine *et al.* 1995). Strains were assayed for radiation sensitivity, genomic DNA was isolated and cleaved with *Eco*RI, and fragments were separated on agarose gels. A Southern blot of the digested DNA was probed with a cosmid containing the *rad50* sequence. The enzyme digest revealed a polymorphism between the radiation-sensitive (*rad12*) and radiation-resistant (wild-type) parent. No recombinants were found in 115 isolates examined, indicating that *rad50* is tightly linked to *rad12*.

A cosmid containing the complete *rad50* gene was used in transformation rescue of the *rad12-4* allele. The cosmid complemented both the radiation sensitivity and the spore formation defects of 34/97 (35%) of the transformants, and 6/97 (6.2%) were complemented for one defect but not both.

Previous work had identified 16 mutants in the *rad12* complementation group (Valentine *et al.* 1995; Table 1). Overlapping fragments of the *rad50* gene were amplified from DNA isolated from all 16 alleles, and mutations were found within the gene for all but one allele. On the basis of the RFLP mapping, complementation, and DNA sequence data, we renamed the *C. cinereus rad12* gene *rad50* and henceforth refer to the gene as *rad50*.

The predicted structures of mutant *C. cinereus* Rad50 proteins: Most *C. cinereus rad50* mutations (Table 1; Figure 1, B and C) are single-base-pair changes resulting in stop codons that truncate the Rad50 protein in the first half of the molecule. The shortest of these predicted mutant proteins is Rad50-11, with a premature stop after amino acid 195, and the longest is Rad50-12, predicted to be 722 amino acids. We found that two alleles, *rad50-1* and *rad50-4*, have mutations in intron splice acceptor sites. For *rad50-1*, genomic sequencing revealed a G to A transition mutation in the AG′ splice acceptor site of intron 4 (supplemental Table S1). We performed RT–PCR using RNA isolated from mushroom caps of a heterokaryotic (*rad50-1* × wild type) strain, cloned the products, and sequenced multiple clones. We found only two types of clones, either wild-type sequences (28/36 clones sequenced) or sequences representing RNAs that had been spliced at the first available AG (italics in supplemental Table S1) after the mutated splice junction (8/36 sequenced clones). The predicted result of the mutation is a Rad50 protein that is normal for 360 amino acids, followed by a 4-amino-acid sequence in which three of four positions are incorrect and then truncation; the resulting protein would be 364 amino acids in length.

Genomic sequencing of *rad50-4* revealed an A to C transversion mutation in the splice acceptor site of intron 20 (Figure 1B and supplemental Figure S1; Table 1 and supplemental Table S1). We sequenced a total of 81 clones from RT–PCR products amplified three separate times from caps of *rad50-4* × wild-type crosses and found that in 24 clones intron 20 was correctly spliced; these clones were expected because the heterokaryotic crosses contained one wild-type allele of *rad50*. For 20 clones, the intron had not been spliced out at all, although upstream and/or downstream introns were spliced in those molecules. The remaining clones revealed three alternatively spliced products. Twenty-one clones had been spliced at the first AG after the normal splice site, 6 had been spliced at the second AG, and 7 had been spliced at the third AG (supplemental Figure S1). Therefore, *rad50-4* is predicted to encode a mixture of mutant proteins. If intron 20 is not spliced at all, the resulting protein is identical to wild type for 1189 amino acids and then has 24 incorrect amino acids before a premature stop. If splicing is at the first AG after the wild-type splice site, the resulting protein has a deletion of 5 amino acids ("VVMTK," aa 1190–1194), if splicing is at the second AG, the protein has a deletion of 7 amino acids ("VVMTKDQ," aa 1190–1196), and if splicing is at the third AG, the protein has 1190 correct amino acids, 11 incorrect amino acids, and then a stop.

Three *rad50* strains have the same mutation, a single T to C transition that results in the substitution of a proline for a leucine at amino acid 742 (Figure 1B; Table 1). The mutants have at least two independent origins; the first, *rad50-5*, was isolated from a screen that was separate from the mutagenesis that generated the other two (Valentine *et al.* 1995). However, it is possible that *rad50-9* and *rad50-10* are actually derived from the same mutagenic event and that the isolate was sampled twice in the screen.

Two other substitution (missense) mutations were found, in *rad50-8* and *rad50-14*, both of which lead to predicted changes within the Walker B box of Rad50 (Figure 1B; Table 1). Rad50-8 has a leucine to serine change at amino acid 1234, and Rad50-14 has an aspartic acid to asparagine change at position 1235. One DNA deletion allele (*rad50-6*) and one insertion allele (*rad50-15*) were also found; *rad50-6* results in an in-frame deletion of eight amino acids within the second coiled-coil domain of Rad50, and *rad50-15* has an insertion of 10 bp (TAC GCA AGG G) at position 2929

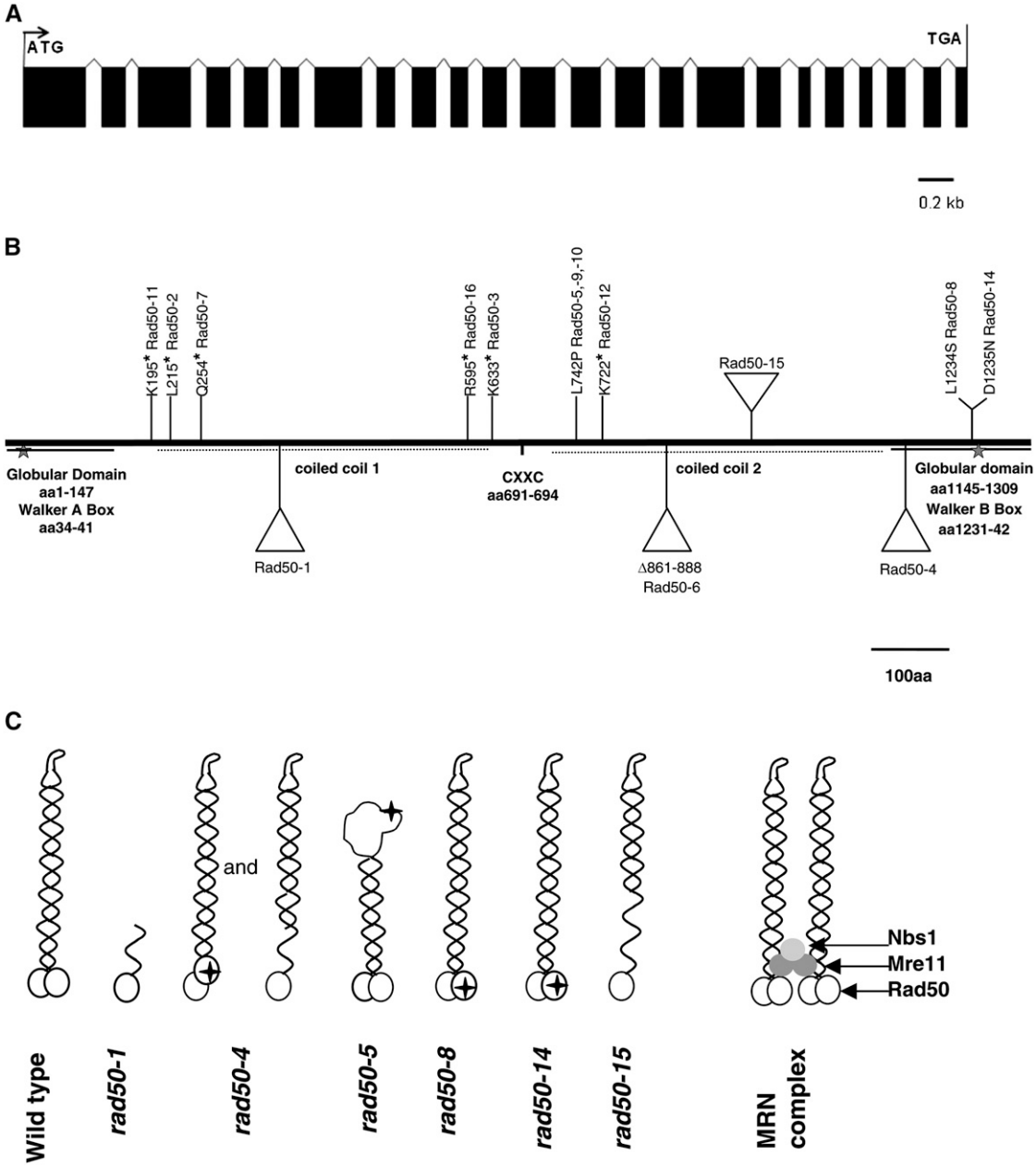

FIGURE 1.—*C. cinereus rad50* gene, protein, and mutants. (A) Gene structure. Solid areas represent exons and open areas represent introns. The translational start site is represented by ATG, and the translational stop is represented by TGA. (B) Rad50 protein and mutations. Stars denote the Walker A and Walker B boxes. Asterisks denote nonsense mutations (stop codons). The Rad50-15 insertion is shown above the protein diagram and the Rad50-1, Rad50-6, and Rad50-4 deletions are shown below. Details of the changes in Rad50-1, Rad50-4, and Rad50-15 are given in Table 1, supplemental Figure S1, and the text. (C) Diagrams of predicted Rad50 mutant proteins. Crosses represent sites of single-amino-acid substitution, or, in the case of Rad50-4, its internal deletion and the altered position of the signature motif. Multiple predicted structures of Rad50-4 are summarized as the two classes that encompass the mutant proteins. Also shown is a model of the MRN complex, as in HOPFNER *et al.* (2002b) and DE JAGER *et al.* (2004).

of the cDNA (Figure 1B; Table 1); the predicted protein is wild type in sequence until amino acid 976 and then has 25 missense amino acids before it ends after amino acid 1001, thus deleting the entire carboxy-terminal globular domain of the protein.

Molecular modeling: Diagrams of predicted Rad50 proteins for alleles studied in depth are shown in Figure 1C. To analyze structural repercussions of mutant Rad50 proteins in more detail, we modeled the predicted effects of the seven-amino-acid deletion in Rad50-4 and of the amino acid substitution in Rad50-5 on the basis of crystal structures of *P. furiosus* Rad50 (Figure 2; HOPFNER *et al.* 2000b). Sequence alignments show the equivalent region encompassing the *C. cinereus*

TABLE 1

***C. cinereus rad50* mutations**

Allele	Mutation		Corresponding amino acid changes[d]	Predicted mutant protein	Meiotic arrest stage
	Position[b]	Codon change[c]			
rad50-1[a]	Intron 4[e]		See text	Truncation	Diffuse diplotene
rad50-2	644	T**T**G > T**A**G	L215*	Truncation	ND
rad50-3	1897	**A**AG > **T**AG	K633*	Truncation	Diffuse diplotene
rad50-7	760	**C**AG > **T**AG	Q254*	Truncation	Diffuse diplotene
rad50-11	583	**A**AA > **T**AA	K195*	Truncation	Diffuse diplotene
rad50-12	2164	**A**AA > **T**AA	K722*	Truncation	ND
rad50-15[a]	2929	+**TAC GCA AGG G**	See text	Truncation	Diffuse diplotene
rad50-16	1783	**C**GA > **T**GA	R595*	Truncation	ND
rad50-4[a]	Intron 20[f]		See text	Internal deletion/ truncation, see text	Diffuse diplotene
rad50-6	Δ2583–2663		Δ861–888	Internal deletion	Diffuse diplotene
rad50-5[a]	2279	C**T**C > C**C**C	L742P	Full-length with disrupted coiled coil	Diffuse diplotene
rad50-9	2279	C**T**C > C**C**C	L742P	Full-length with disrupted coiled coil	Diffuse diplotene
rad50-10	2279	C**T**C > C**C**C	L742P	Full-length with disrupted coiled coil	Diffuse diplotene
rad50-8[a]	850	(aa**a** > aa**g**)	(K284K) L1234S	Single-site substitution	Metaphase-like
	3701	T**T**A > T**C**A			
rad50-14[a]	3703	**G**AT > **A**AT	D1235N	Single-site substitution	Diffuse diplotene
rad50-13	No change found				ND

ND, not determined.
[a] Alleles studied in depth and shown in Figure 1C.
[b] All positions refer to nucleotides of the coding strand of the open reading frame except where indicated.
[c] Nucleotide changes are in boldface type.
[d] Single-letter amino acid designations are used. An asterisk denotes a stop codon.
[e] The end of intron 4's sequence is changed from CA**G** to CA**A** in *rad50-1*.
[f] The end of intron 20's sequence is changed from T**A**G to T**C**G in *rad50-4*.

Rad50-4 deletion maps to *P. furiosus* Rad50 β-sheet β9 (Figure 2, A and B). In the ATP-bound structure of *P. furiosus* Rad50, sheets β9 and β10 and the neighboring Rad50 ABC signature motif directly participate in formation of the ATP binding pocket and the nucleotide-mediated Rad50 dimerization interface. When deleted in the *rad50-4* mutant, removal of β9 likely causes destabilization of the β8-β9-β10 sheet, disruption of the signature motif, and distortion of the ATP binding pocket (Figure 2, A and B). The signature motif is critical for Rad50 dimerization and for MRN complex DNA binding (Hopfner *et al.* 2002b). A signature motif mutation in *P. furiosus* Rad50 protein was found to dramatically lower ATP binding (Moncalian *et al.* 2004); however, equivalent mutations in the *S. cerevisiae* and human proteins are defective in adenylate kinase activity but not ATP binding or hydrolysis (Bhaskara *et al.* 2007).

The Rad50-5 mutation, a leucine to proline substitution, occurs at the beginning of the second coiled-coil domain of the protein (Table 1; Figures 1B and 2D). This is predicted to result in partial or complete destabilization of the portion of the coil just after the hook domain (Figure 2C).

Meiotic defects in *rad50* mutants: *Spore viability of rad50 mutants and heterozygotes:* Because Rad50 functions as a multimer (Hopfner *et al.* 2000b), the *rad50-1*, *rad50-4*, *rad50-5*, *rad50-8*, and *rad50-15* mutants were assessed for dominance using a spore viability assay of homozygous (homokaryotic) *vs.* heterozygous (heterokaryotic) strains. Five experiments were performed for each strain, at least 200 spores were scored for each experiment, and spore viabilities were averaged. Spore viability for the wild-type strain, J6;5x4, was 87.8%. Mutant strains *rad50-1*, *rad50-4*, *rad50-5*, *rad50-8*, and *rad50-15* had average spore viabilities of 2.0, 4.4, 3.8, 18.7, and 16.7%, respectively. The heterokaryons of *rad50-1*, *rad50-4*, *rad50-5*, *rad50-8*, and *rad50-15*, in each case crossed to wild type, gave spore viabilities of 78.8, 80.4, 79.9, 89.3, and 80.1%, values that exhibited no statistically significant difference from wild-type mushrooms (ANOVA analysis; *P*-value >0.05).

Diffuse diplotene arrest of rad50 mutants: Meiosis in *C. cinereus* is synchronous and takes ~12 hr from karyogamy through the second meiotic division (Raju and Lu 1970; Pukkila *et al.* 1984). At 6 hr after karyogamy (K + 6), essentially all meiotic cells in the mushroom cap are in pachytene (Pukkila *et al.* 1984; Seitz *et al.*

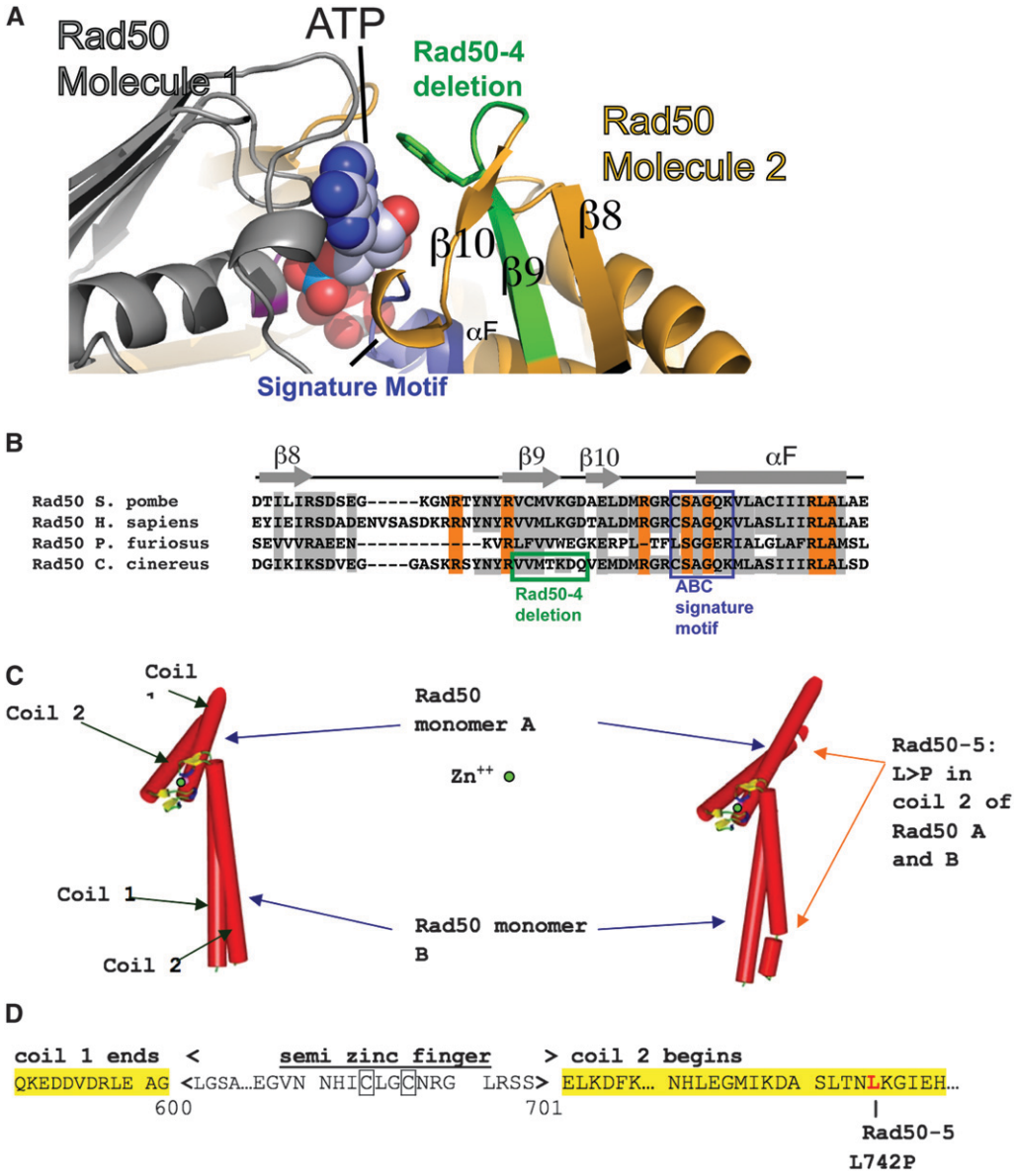

FIGURE 2.—Molecular models of *C. cinereus* Rad50. (A) The Rad50-4 deletion removes sheet β9, and the β9–β10 connecting loop, thereby disrupting the Rad50 ATP binding and dimerization interaction site. Ribbon models are based upon homology with the *Pyrococcus furiosus* Rad50 protein. (B) Alignment of the β9 and signature motif regions of *P. furiosus*, *C. cinereus*, *S. pombe*, and *H. sapiens* Rad50. The green-highlighted amino acids are deleted in one splicing variant of Rad50-4; in another, the five amino acids VVMTK are deleted. The ABC signature motifs are boxed in purple. (C) Rod model of the hook and part of the coiled-coil regions of wild-type Rad50 and Rad50-5. (D) A portion of the Rad50 protein sequence, showing the region mutated in Rad50-5.

1996); homologous chromosomes are fully condensed and paired, and the SC is fully developed. At ~8 hr after karyogamy (K + 8), cells enter diffuse diplotene. At this stage, the SC has dissipated, and chromosomes are diffuse in appearance. Nine to 10 hr after karyogamy (K + 10) chromosomes undergo a second condensation and enter metaphase I, and by 12 hr after karyogamy (K + 12) all basidia have completed both meiotic divisions and contain a tetrad of haploid nuclei (Figure 3A).

Previous analysis of chromosome spreads of *rad50-1*, *rad50-4*, and *rad50-15* (RAMESH and ZOLAN 1995) showed that they undergo karyogamy 30–60 min later than wild-type strains but are similar to wild-type strains in the timing of the formation and dissolution of AEs and SC during meiosis. That is, although *rad50* mutants do not achieve complete SC formation (*i.e.*, pachytene), the timing of maximal AE and SC formation is comparable to that of wild type, and the AEs and SCs that do form then disperse at times similar to that of wild type. However, we also found that *rad50* mutants arrest in diffuse diplotene. We extended this study within our collection of *rad50* mutants and examined single-layer gill segments taken from mushrooms at K + 12 (Table 1). We found that all *rad50* mutants examined apparently arrest at diffuse diplotene except for *rad50-8* (Figure 3A). The majority of basidia in *rad50-8* arrest at metaphase I in a spindle-like shape, which implies that this mutant progresses farther through meiosis. To examine *rad50* arrest in more detail, we stained arrested tissue from *rad50-4* with both DAPI and an antibody against α-tubulin (Figure 3B). We found that 43% of the cells arrested with larger discs of chromatin and that these were without organized spindles, while 57% of cells had more compact DAPI-staining discs and spindle-shaped microtubule organization ($n = 60$). Therefore, the *rad50-4* arrest phenotype is actually a

mixture of two distinct, arrested cell types, probably corresponding to diffuse diplotene and condensed chromatin entering metaphase I. The *rad50-8* allele allows all cells to progress to the metaphase I-like state.

The spo11-1 mutation is epistatic to rad50 mutations and mre11-1 for meiotic arrest: In *S. cerevisiae*, most *rad50* mutants are phenotypically similar to *spo11* null mutants, in that meiotic DSBs are not formed. However, in *rad50S* mutants (Alani *et al.* 1990), DSBs are made but not processed; Spo11 protein remains bound to the 5′ ends of the DSB (Keeney *et al.* 1997). In *C. cinereus*, the *spo11-1* mutant is likely defective at DSB formation, because gamma irradiation of mushrooms partially suppresses the mutant's meiotic defects (Celerin *et al.* 2000); in addition, Rad51 foci are not induced during meiosis in *spo11-1* (Figure 4F; supplemental Figures S3 and S4). In *spo11-1*, meiotic cells progress into an aberrant, metaphase I-like stage and then undergo programmed cell death (PCD) (Figure 3C; Celerin *et al.* 2000). In contrast, *rad50* mutants remain arrested in either diffuse diplotene or a metaphase I-like state for several hours (Ramesh and Zolan 1995; Figure 3A).

We thought it possible that the *C. cinereus rad50* mutants were all permissive for meiotic DSB formation but defective in DSB processing. If this were the case, then *spo11-1*, which does not make meiotic DSBs, would be epistatic to *rad50* mutations. To test this prediction, we constructed *rad50;spo11-1* double mutants and found that they underwent signature PCD chromatin changes characteristic of the *spo11-1* single mutant (data for the *rad50-4* and *rad50-8* mutants are shown in Figure 3C; similar results were obtained for *rad50-5*). This result indicated that Spo11 has activity in *rad50* mutants and that this activity is required for the *rad50* mutant arrest. In a previous study, we found that *mre11-1* arrests variably at diffuse diplotene or in a metaphase I-like state (Gerecke and Zolan 2000). We constructed an *mre11-1;spo11-1* double mutant and found that it also exhibited a *spo11-1* PCD phenotype, indicating that *spo11-1* PCD is epistatic to the *mre11-1* arrest phenotype (Figure 3D). Therefore, Spo11 likely functions before both Mre11 and Rad50 in *C. cinereus* meiosis; this observation also implies that Spo11-catalyzed DSB formation may be MRN complex independent in *C. cinereus*.

Rad51 foci are induced during meiosis for some rad50 alleles: We reasoned that if Spo11 forms DSBs in *C. cinereus* MRN complex mutants, then the array of Rad50 mutant proteins in our alleles might vary in their ability to process those breaks and succeed with recombination-dependent events of prophase I. As shown in *S. cerevisiae* (reviewed in Keeney 2008), break formation is followed by MRN complex-dependent processing, which removes Spo11 from the 5′ ends of the breaks and asymmetrically forms single-strand ends that bind Rad51 and Dmc1 and invade a nonsister chromatid. To investigate recombination events in *C. cinereus*, we raised and purified antibody against full-length Rad51 protein (supplemental Figures S2–S4) and used it to examine the time course of Rad51 focus formation during meiosis in a wild-type dikaryon (Figure 4). We found that Rad51 foci are induced after karyogamy and peak in number at K + 4 and K + 6, corresponding to the zygotene and pachytene stages of prophase I, and our results are similar to those obtained previously using immunofluorescence staining of *C. cinereus* tissue sections with an independently derived anti-Rad51 antibody (Nara *et al.* 2001). In contrast, Rad51 foci are not induced during meiosis in *spo11-1* (Figure 4F; supplemental Figures S3 and S4), in which the number of foci was not significantly different from that seen in wild type before and during karyogamy (in two-sample *t*-tests: K − 1, $P = 0.830$; K + 0, $P = 0.258$), and remained essentially constant throughout prophase I. Our results with *spo11-1* are similar to those reported for Dmc1 by Holzen *et al.* (2006), who found a low, residual number of foci in an *S. cerevisiae spo11* mutant.

To compare wild-type and mutant strains, we examined Rad51 foci at K + 4 in *mre11-1* and an array of *rad50* mutants. We found that mutant strains fell into two clear classes (Figure 5A). The first, which includes *mre11-1*, *rad50-1*, *rad50-4*, and *rad50-5*, formed numbers of foci that were not significantly different from that found in *spo11-1*. The second class of mutants, *rad50-8*, *rad50-14*, and *rad50-15*, formed significantly greater numbers of Rad51 foci than *spo11-1*, although significantly fewer foci than wild type. These three strains were examined further for the timing of Rad51 focus formation. In *rad50-14*, the number of foci increased at later meiotic stages, to levels greater than that of wild type by K + 8 (Figure 5B). For both *rad50-8* and *rad50-15*, early meiotic time points showed higher than wild-type levels of foci at K + 1 and then a decrease in foci to an intermediate level by K + 4 (data for *rad50-15* are shown in Figure 5B). For *rad50-15*, we further examined its time course by staining samples taken before karyogamy (K − 1 and K + 0), to examine the initial appearance of foci, and at K + 6 and K + 8, to determine whether the number of foci remains constant at these later time points (Figure 5B). At K − 1 and K + 0, the numbers of Rad51 foci in a *rad50-15* strain were not significantly different from those in either *spo11-1* or wild type (ANOVA, $P = 0.107$ at K − 1 and $P = 0.330$ at K + 0). This indicates that the increase in foci seen in *rad50-15* at K + 1 is occurring in response to breaks formed during meiotic prophase and not during the karyogamy or premeiotic S phases. Examination of the later time points showed a persistent level of foci, likely indicating that unresolved recombination events remained.

If Rad51 foci in *rad50* mutants are meiosis specific, they should be Spo11 dependent. As predicted, a *rad50-8; spo11-1* double mutant examined at K + 6 had significantly fewer foci (22.9 ± 3.0) than that observed in *rad50-8*, *rad50-14*, or *rad50-15* at any time point ($P < 0.001$).

Synaptonemal complex formation in rad50 mutants: To characterize SC formation in *rad50* mutants, we examined

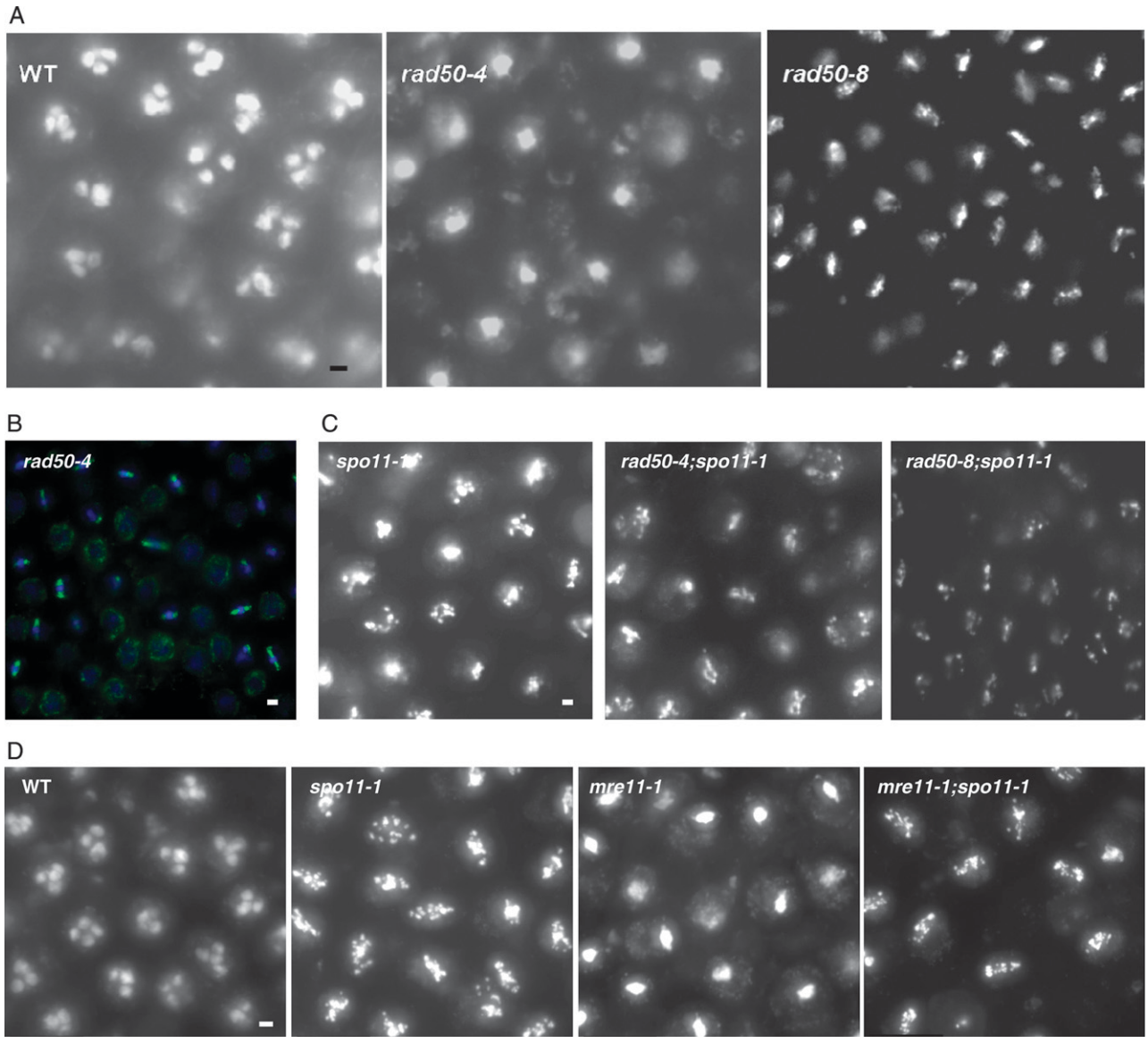

FIGURE 3.—*rad50* mutant and *mre11-1* arrests are Spo11 dependent. (A–C) Samples were taken from mushrooms 12 hr after karyogamy, fixed, stained with DAPI, and photographed. (A) Wild-type and *rad50-4* and *rad50-8* single mutants. (B) *rad50-4* stained with DAPI and with spindles detected using mouse anti-α-tubulin antibody, as described in CELERIN *et al.* (2000). (C) A *spo11-1* single mutant compared with *rad50-4;spo11-1* and *rad50-8;spo11-1* double mutants. (D) Wild-type, *spo11-1*, and *mre11-1* single mutants compared to *mre11-1;spo11-1*. Tissue samples, taken at K + 10, were stained with DAPI and photographed as a *z*-stack series of images. Image stacks were flattened into a single image as described in the text. Bars, 2 μm.

electron micrographs of silver-stained surface-spread nuclei. The three *rad50* alleles found to be defective for Rad51 focus formation, *rad50-1*, *rad50-4*, and *rad50-5* (Figure 5A), were also severely deficient for SC formation (Figures 6 and 7); the SC data for *rad50-1* and *rad50-4* are similar to those we previously reported (RAMESH and ZOLAN 1995). In contrast, the three *rad50* alleles with significantly more Rad51 foci than *spo11-1*, *rad50-8*, *rad50-14*, and *rad50-15* formed more AEs and SCs than the severely defective alleles (Figure 6). The allele *rad50-15* had previously been examined after one outcross generation (RAMESH and ZOLAN 1995), and our results were similar to those previously obtained.

Homolog pairing: The concordance between elevated (relative to *spo11-1*) numbers of Rad51 foci and elevated SC formation for *rad50-8*, *rad50-14*, and *rad50-15* led us to ask whether stable homolog pairing correlates with these indicators of recombination activity. We used FISH (LI *et al.* 1999) to examine the extent of meiotic pairing on two sites on chromosome 13, one telomeric and one interstitial, for *rad50-1*, *rad50-5*, *rad50-8*, and *rad50-14* (Table 2). The data for *rad50-1* were similar to those obtained previously for *mre11-1* (GERECKE and ZOLAN 2000) and those we obtained for *spo11-1*; ~25% of nuclei showed pairing for both probes at K + 6. In contrast, *rad50-5* had less pairing than any other strain;

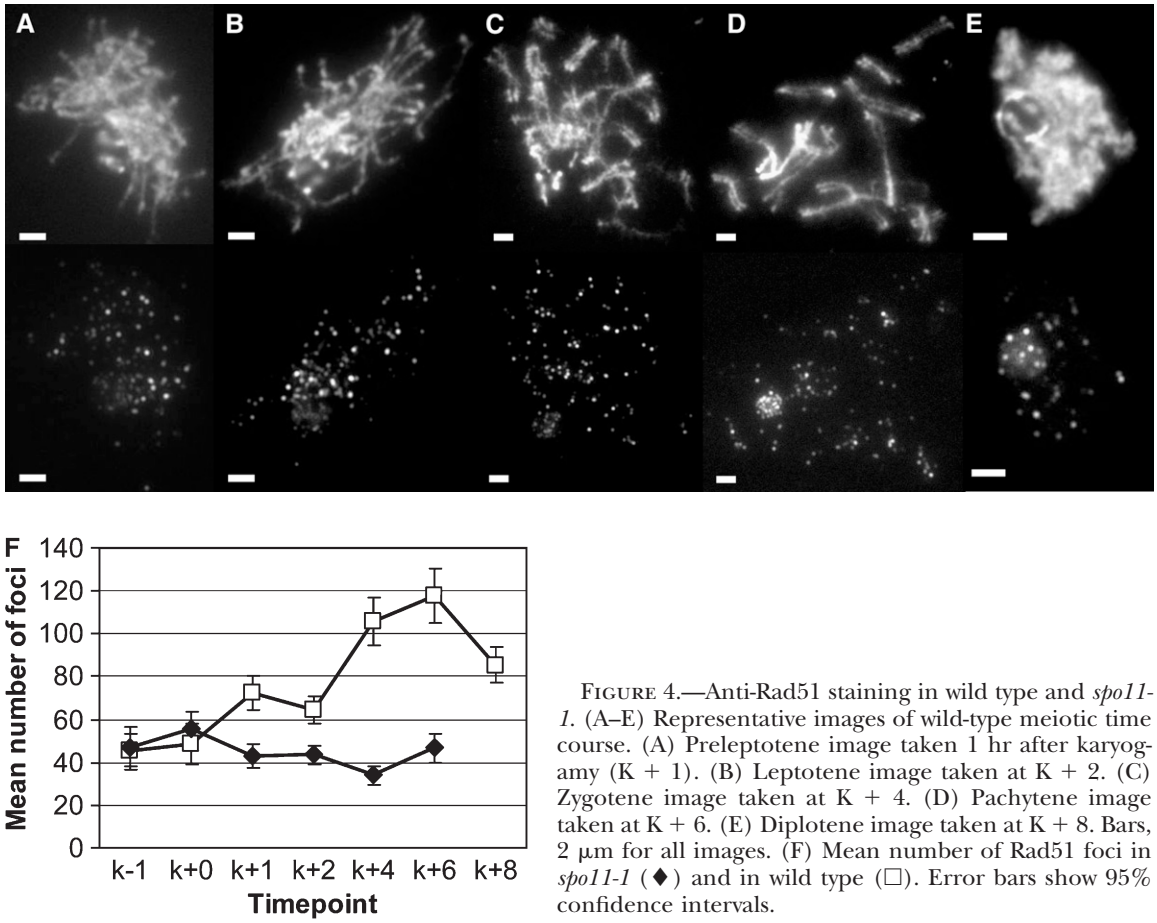

FIGURE 4.—Anti-Rad51 staining in wild type and *spo11-1*. (A–E) Representative images of wild-type meiotic time course. (A) Preleptotene image taken 1 hr after karyogamy (K + 1). (B) Leptotene image taken at K + 2. (C) Zygotene image taken at K + 4. (D) Pachytene image taken at K + 6. (E) Diplotene image taken at K + 8. Bars, 2 μm for all images. (F) Mean number of Rad51 foci in *spo11-1* (♦) and in wild type (□). Error bars show 95% confidence intervals.

only 13% of nuclei had both loci paired at K + 1, and only 6% had both loci paired at K + 6.

The *rad50* strains that had some partial recombination activity exhibited a higher amount of pairing at K + 6 (*rad50-8*, 36%; *rad50-14*, 40%) than *rad50-1* (24%), although with our data set this difference is not statistically significant ($P = 0.202$ for the *rad50-8* comparison with *rad50-1* and $P = 0.096$ for the *rad50-14* comparison).

Because we used both a telomere-proximal probe (LI *et al.* 1999) and an interstitial probe, we were able to examine differences in pairing on the same chromosome. For the *rad50-1* strain we observed a greater amount of pairing with the interstitial probe as compared to the telomeric probe. This difference was significant at K + 1 (70% compared to 33%; chi-square test, $P < 0.001$), but was not significant at K + 6 ($P = 0.342$). In addition, none of the other *rad50* mutants examined showed a significant difference in percentage of pairing between the two probes at any time point.

Analysis of AE formation in rad50 mutants: Most studies of Rad50 have focused on mutations that affect the catalytic activities of the MRN complex. In addition, the hook portion of the Rad50 protein has been shown to be of critical importance in both intracomplex and intercomplex interactions (HOPFNER *et al.* 2002a) and in the *in vivo* functions of the complex (WILTZIUS *et al.* 2005). We were interested in separating the functions of Rad50 in meiotic DSB formation and processing from any structural role the protein may have in meiosis. Therefore, we investigated AE formation by *rad50* mutants in the *spo11-1* background, in which DSBs are not made.

Using *rad50;spo11-1* double mutants and sibling progeny that were single mutants for each gene or wild type, we generated electron micrographs of silver-stained, surface-spread meiotic nuclei and scored each strain for AE and SC formation (Figure 7; Table 3). AE and SC lengths were measured from nuclear spreads taken from one mushroom of each strain (data for *rad50-4* and *rad50-5* are shown in Figure 7, B and D).

As expected and as previously reported for other *spo11-1* strains (CELERIN *et al.* 2000), nuclei from the *spo11-1* single mutants showed either no structure or AE formation only (Figure 7; Table 3). The number of AE segments and their lengths in those *spo11-1* nuclei that formed AEs were variable, with 5 to 42 AE segments forming per nucleus, individual AE lengths ranging from 0.3 to 20 μm, per nucleus lengths ranging from 12 to 173 μm, and overall AE length per nucleus ranging from 12 to 206 μm. The average AE lengths per nucleus for the two *spo11-1* strains shown in Figure 7, A and C,

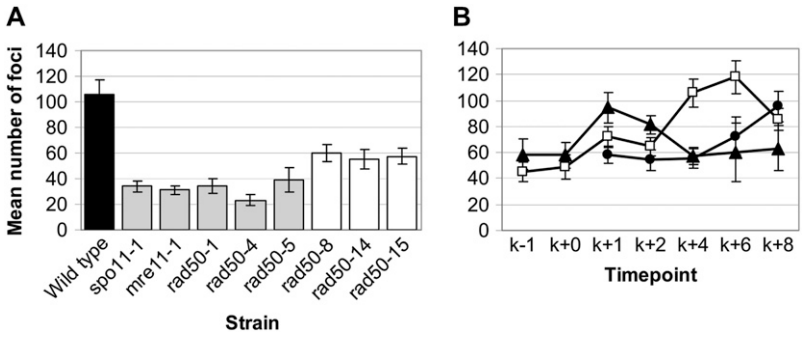

FIGURE 5.—Mutants fall into two classes for Rad51 focus formation. (A) Mean number of Rad51 foci observed at K + 4. (B) Time course of Rad51 foci in *rad50-14* and *rad50-15*. Wild-type data (□) are the same as in Figure 4 and shown for reference. ●, *rad50-14*; ▲, rad50-15. Error bars show 95% confidence intervals.

were 73 and 126 μm, respectively. For comparison, a congenic wild-type strain consistently formed 26 AEs, with an average AE length per nucleus of 124 μm. Although the *rad50-1*, *rad50-4*, and *rad50-5* single mutants were similar to one another, the *rad50-4;spo11-1* double mutant was strikingly different from the *rad50-1;spo11-1* and *rad50-5;spo11-1* double mutants (Figure 7; Table 3). We found that the presence of Rad50-4 was sufficient for the formation of long AE's in a *spo11-1* mutant background (Figure 7, A and B). For those nuclei that formed AE, the number of AE segments ranged from 17 to 40, and the average AE length per nucleus was 153 μm. However, in both the *rad50-1;spo11-1* and the *rad50-5;spo11-1* double mutants, little AEs was found.

Chi-square analysis showed that for *rad50-4;spo11-1*, the distribution of nuclei into classes with chromosome structures (AE and/or SC) and without structure was the same as for *spo11-1* ($P = 0.116$). In contrast, for both *rad50-1;spo11-1* and *rad50-5;spo11-1*, the distributions of nuclei in the two categories were significantly different from that of the sibling *spo11-1* strain and in all but one case not significantly different from that of the sibling *rad50* single mutant. For *rad50-1*, progeny from one cross to *spo11-1* were examined (Table 3, cross B), and the *rad50-1;spo11-1* double mutant was different from *spo11-1* ($P = 0.018$) and the same as *rad50-1* ($P = 0.322$). For *rad50-5*, two different crosses were examined (Table 3, crosses C and D). For progeny from the first cross, the *rad50-5;spo11-1* double mutant was significantly different from *spo11-1* ($P < 0.001$) and not different from the *rad50-5* single mutant ($P = 0.322$). For cross D, two different *rad50-5;spo11-1* double mutants were examined. The first (48 × 6) was significantly different from *spo11-1* ($P < 0.001$) and the same as *rad50-5* ($P = 0.754$). The second (40 × 70) was significantly different from *spo11-1* ($P = 0.047$) but also significantly different from the sibling *rad50-5* strain examined ($P = 0.007$). Overall, our data show that the disruption (in Rad50-5) or absence (in Rad50-1) of the Rad50 hook-proximal coiled coil makes the formation of stable AE unlikely. Our results indicate that there is a structural role for Rad50, separate from the DSB-processing activity of the MRN complex, which is required for the formation of meiotic chromosome structures.

DISCUSSION

***C. cinereus rad50* mutations are recessive:** For proteins that normally function as multimers, mutants that can assemble into complexes often exhibit dominant-negative phenotypes in heterozygotes (HERSKOWITZ 1987). Because of the known structure of the Mre11/Rad50 complex, we expected that at least some *rad50* alleles would behave as dominant negatives. However, heterokaryon spore viabilities did not show statistically significant differences from wild-type spore viabilities, indicating that the *rad50* mutations examined (*rad50-1*, *rad50-4*, *rad50-5*, *rad50-8*, and *rad50-15*) are not dominant. A simple explanation for this would be instability of all mutant Rad50 proteins. However, the phenotypes of a number of *rad50* mutants are distinct (*e.g.*, Figure 4; RAMESH and ZOLAN 1995); therefore, at least some of them make stable protein. In addition, recent studies have shown that Rad50-5 forms foci on meiotic chromosomes (A. MANY, C. MELKI, D. MAILLET, S. ACHARYA and M. ZOLAN, unpublished results). Therefore, although it is possible or even likely that some alleles (*e.g.*, *rad50-1*) encode unstable protein, the recessive nature of all *rad50* mutations examined cannot be explained by a simple absence of stable protein. It is possible that none of the mutant proteins can form sufficiently stable dimers with wild-type Rad50 to become incorporated into complete MRN complexes or to diminish the pool of wild-type complexes. In any case, the pool of fully functional MRN is sufficient in the heterokaryons for the production of viable meiotic products, although subtle effects on meiosis (*e.g.*, on crossover frequency or distribution) would not have been detected by our analysis.

***C. cinereus rad50* mutants form meiotic DSBs:** In *rad50;spo11-1* and *mre11-1;spo11-1* double mutants, the *spo11-1* PCD phenotype is epistatic to the *rad50* or *mre11-1* phenotype, in all allele combinations examined (Figure 3 and data not shown). Therefore, our data imply that Spo11 has activity in *rad50* and *mre11* mutants. Although Spo11 has meiotic functions that are independent of its DSB-forming activity (*e.g.*, CHA *et al.* 2000), the *spo11-1* single mutant forms essentially no SC (CELERIN *et al.* 2000), whereas *rad50* and *mre11*

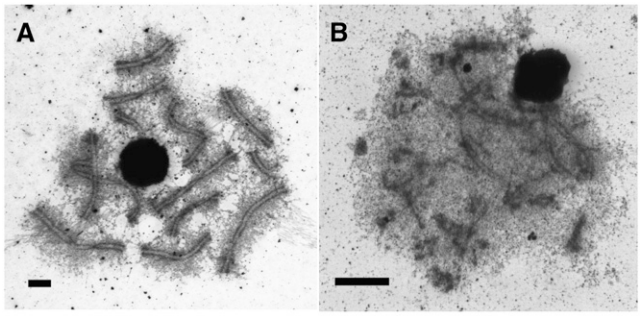

C

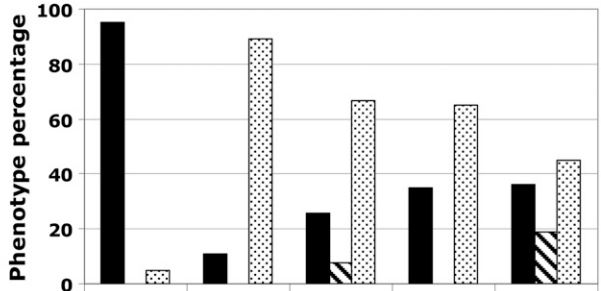

	Wild type	rad50 -1	rad50 -8	rad50 -14	rad50 -15
SC	95.0	11.0	25.6	35.1	36.0
AE only	0.0	0.0	7.7	0.0	19.0
Neither	5.0	89.0	66.7	64.9	45.0

Figure 6.—SC formation in wild type, *rad50-8*, *rad50-14*, and *rad50-15*. Surface spreads of wild-type (A) and *rad50-14* (B) nuclei from the K + 6 time point were stained with silver nitrate and photographed using transmission electron microscopy. Bars, 2 μm for all images. (C) Percentage of SC and AE formation for each strain. The number of images categorized was as follows: wild type, 40; *rad50-8*, 78; *rad50-14*, 57; *rad50-15*, 100.

mutants form SC in variable amounts (Ramesh and Zolan 1995; Gerecke and Zolan 2000; this work). As discussed recently by Borde (2007), the partial SC formation in *C. cinereus rad50* and *mre11* mutants is similar to that seen in those *S. cerevisiae* MRN mutants (such as *rad50S*; Alani *et al.* 1990) in which Spo11 forms but does not process meiotic DSBs (Keeney *et al.* 1997). In addition, like *S. cerevisiae rad50S* (Gasior *et al.* 1998), some of the *C. cinereus rad50* alleles form Rad51 foci at levels lower than that observed in wild-type strains but significantly higher than that found for *spo11-1* (Figure 5). Because the Rad51 foci correlate in the *rad50* alleles with enhanced levels of stable homolog pairing and SC formation (relative to *spo11-1*; Figure 6 and Table 2), and because they are Spo11-dependent, at least a portion of them must represent progression through a normal meiotic program of Spo11-dependent DSB processing, leading to synapsis (Kleckner 2006).

For the *rad50* alleles that formed Rad51 foci, the time courses of focus formation and loss were different from that of the wild-type strain examined (Figure 5B). For *rad50-14*, the number of Rad51 foci increased at time points corresponding to late prophase in wild-type strains. The predicted Rad50-14 protein has an aspartate to asparagine substitution in the Walker B domain (Figure 1B; Table 1), which might result in DSB processing that is stalled or delayed compared to that in wild-type cells. An alternative possibility is that these late events may not be related to Spo11-induced DSBs but may be repair events resulting from the accumulation of DNA damage as the cells attempt to proceed through meiotic prophase. For *rad50-8* and *rad50-15*, we found that a large number of foci are observed at K + 1 and decrease thereafter. One simple interpretation of this is that these foci mark recombination events in which an aberrant processing step occurs soon after the formation of meiotic DSBs, followed by disassociation of the MRN complex.

Because all of the *rad50* mutants, and *mre11-1* arrest in meiosis, because this arrest is Spo11 dependent (Figure 3), and because some of the alleles form inducible, Spo11-dependent Rad51 foci (Figure 5) and therefore must be forming DSBs, we think it likely that arrest in both *mre11-1* and the collection of *rad50* mutants is the result of unrepaired or improperly processed DSBs in the genome and that Rad50 and Mre11 are dispensable for DSB formation in *C. cinereus*, but required for appropriate DSB processing. This interpretation assumes that truncation alleles (*e.g.*, *rad50-1* and *mre11-1*) in fact encode unstable protein. Alternatively, the Walker A box alone of Rad50 and the N-terminal 40% of Mre11 are sufficient to allow formation, but not complete and/or proper processing, of meiotic DSBs. Although *S. cerevisiae rad50* and *mre11* null or deletion mutants show no meiotic DSB formation, as assayed by pulsed-field gel analysis of genomic DNA (Cao *et al.* 1990; Nairz and Klein 1997), *rad50* deletion mutants of *S. pombe* do form meiotic DSBs (Young *et al.* 2004). In addition, Spo11 has DSB-forming activity in *mre11* mutants of *S. pombe* (Young *et al.* 2004) and *A. thaliana* (Puizina *et al.* 2004). In *C. elegans*, Rad50 facilitates DSB formation by Spo11, but Rad50 is apparently not strictly required for Spo11 activity, because a defect in a cohesin protein, Rec8, allows Spo11-dependent DSB formation in the absence of Rad50 function (Hayashi *et al.* 2007). Thus, *S. cerevisiae* may be the exception, rather than the rule, in its requirement for the MRN complex in meiotic DSB formation.

Rad50's structural roles in meiosis: The *C. cinereus rad50* mutants undergo varying amounts of AE and SC formation, and a comparison of the predicted Rad50 structures (Figures 1 and 2) with the meiotic phenotypes of the mutants (Ramesh and Zolan 1995; Figure 4) is informative. Three alleles, *rad50-1*, *rad50-4*, and *rad50-5*, are comparably severe as single mutants (except in homolog pairing, discussed below). Because *rad50-1* encodes a severely truncated protein, it is not surprising that little function is retained, and this allele is most likely effectively null. For Rad50-4, modeling revealed that the loss of a β-strand (Figure 2A) likely

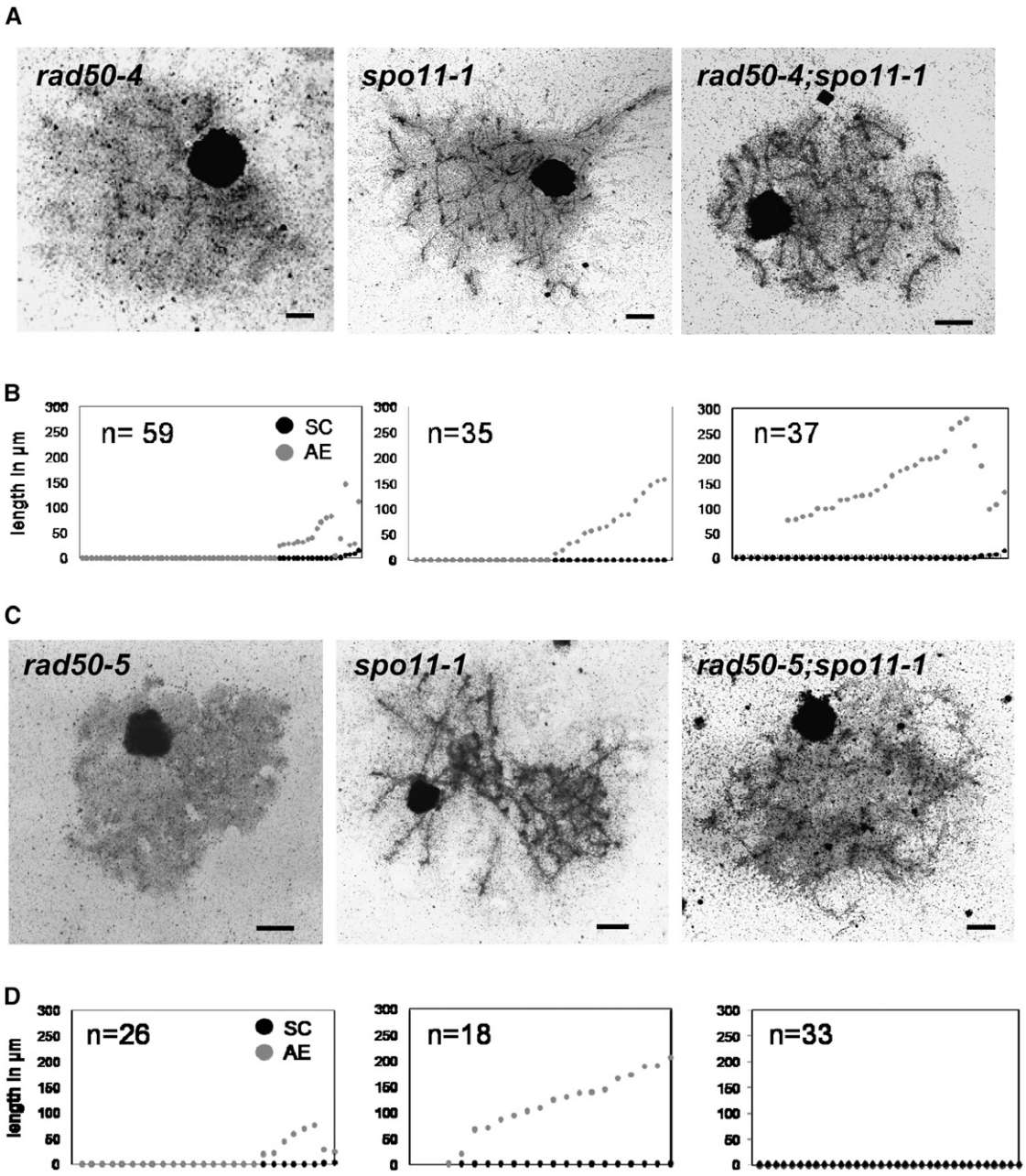

Figure 7.—The coiled coil of Rad50 proximal to the hook is required for AE formation. (A and C) Samples were taken at 6 hr after karyogamy, fixed, spread, and stained and photographed using EM as described (Seitz *et al.* 1996). (B and D) Data from nuclear spreads from a single mushroom were plotted according to increasing SC length. Each graph corresponds to the genotype shown in the image above it. Images were chosen to represent the major class of nuclear spreads observed for each genotype. Bars, 2 μm.

distorts the ATP binding pocket and neighboring signature motif. The signature motif (in the C-terminal globular domain) of Rad50-4 may not be in the correct orientation for contact with the ATP bound to the N-terminal domain of another Rad50-4. This may result in a loss of Rad50 head domain dimerization (Moncalian *et al.* 2004). In addition, the signature motif is essential for the recently reported and essential adenylate kinase activity of *S. cerevisiae* Rad50 (Bhaskara *et al.* 2007) and may be abrogated in Rad50-4 molecules. Also, because the deletion is at the junction where the Rad50 globular ATPase domain adjoins the coiled coil, it may affect coil stability in this region and therefore Mre11 binding (Hopfner *et al.* 2001). An unspliced *rad50-4* transcript is predicted to make a protein similar to Rad50-15, and transcripts containing an unspliced intron composed about one-third of the mutant cDNAs examined. Given that there is a mix of aberrantly spliced transcripts in the *rad50-4* mutant, it is perhaps surprising that only the severe phenotype prevails. It may be that there is

TABLE 2

Homolog pairing

Strain	Time point	*N*	% pairing: Interstitial probe	Telomeric probe	Both probes	Either probe
Wild type	K + 1	82	78	72	60	90
Wild type	K + 6	39	90	92	82	100
spo11-1	K + 6	39	33	49	26	56
rad50-1	K + 1	40	70	33	23	80
rad50-1	K + 6	37	51	43	24	70
rad50-5	K + 1	45	27	20	13	33
rad50-5	K + 6	68	24	15	6	32
rad50-8	K + 6	83	43	43	36	51
rad50-14	K + 6	93	52	49	40	61

Data are arrayed by time point and strain. For each combination of time point and strain at least two experiments, examining two different mushrooms, were performed. Data shown combine images from all experiments on a given time point and strain.

TABLE 3

Effect of hook-proximal coiled-coil structure on AE and SC formation

Strain[a]	% SC[b]	% AE	% no structure	Total (*N*)
Cross A: *rad50-4* × *spo11-1*				
rad50-4 11 × 30	6	15	79	79
spo11-1 93 × 44	0	43	57	62
rad50-4;spo11-1 18 × 12	7	49	44	120
Cross B: *rad50-1* × *spo11-1*				
rad50-1 96 × 13	11	0	89	75
spo11-1 195 × 176	0	45	55	55
rad50-1;spo11-1 47 × 59	0	21	79	34
Cross C: *rad50-5* × *spo11-1*				
rad50-5 19 × 45	0	4	96	137
spo11-1 7 × 29	7	48	44	81
rad50-5;spo11-1 59 × 21	0	7	93	75
Cross D: *rad50-5* × *spo11-1*				
rad50-5 60 × 69	2	8	90	137
spo11-1 35 × 50	0	30	70	169
rad50-5;spo11-1 48 × 6	1	8	91	248
rad50-5;spo11-1 40 × 70	7	14	78	222

[a] Strains used were dikaryons formed by crosses between the indicated, numbered, sibling monokaryons.

[b] For some crosses, percentages do not sum to 100 due to rounding.

insufficient truncated, Rad50-15-like protein to allow SC formation in *rad50-4*.

The *rad50-5* mutation causes a leucine to proline change at the beginning of the second coil (Figures 1 and 2, C and D). From modeling, it is predicted to result in either an interruption or a distortion of the second coil. The stability of coiled-coil structures and their segmented structure (M. Oakley, personal communication) predicts that only the beginning of the coiled-coil region, and probably the hook region, is affected in Rad50-5. Therefore, it is striking that the meiotic defects in *rad50-5* strains are as severe as those caused by the *rad50-1* allele and, in fact, that homolog pairing is worse in *rad50-5* than in *rad50-1* or *spo11-1* (Table 2). The analysis of Wiltzius *et al.* (2005) showed that the hook region of *S. cerevisiae* Rad50 is essential for DNA repair and meiotic DSB formation. Our data show that this region is also essential for the formation of stable AEs and SCs.

The requirement for the hook-proximal coiled coil of Rad50 in stable AE formation is shown dramatically by our analysis of AE formation in *rad50;spo11-1* double mutants (Figure 7). For *rad50-4*, the *spo11-1* mutation seems to be fully epistatic; the *rad50-4;spo11-1* double mutant is the same as *spo11-1* for both PCD (Figure 3) and AE formation (Figure 7; Table 3). In contrast, the *spo11-1* phenotype of variable AE formation is masked, in *rad50-1* and *rad50-5* strains, by the inability of those mutants, even in the *spo11-1* background, to form stable AEs. Therefore, Rad50 has a structural role in AE formation that must be independent of its role in processing Spo11-catalyzed DSBs.

In contrast with *rad50-1*, *rad50-4*, and *rad50-5*, the *rad50-15* mutant makes extensive AEs and SCs. This allele contains an insertion that leads to the production of a protein with 25 incorrect amino acids after position 976, followed by a stop (Table 1 and Figure 1, B and C). The Walker A box is intact and the coiled domains presumably fold normally, but the globular domain containing the Walker B motif is missing. Since the Walker B motif is absent, and this mutant is radiation sensitive, it is unlikely that Rad50-15 is catalytically active. Similarly, *rad50-8* and *rad50-14* have mutations within the Walker B region, which should abrogate or at least diminish function. The phenotypes of these mutants imply that AE and SC formation are to a large extent independent of Rad50's ATPase or adenylate kinase functions. Instead, the main role of Rad50 in meiotic DSB processing may be via its interaction with Mre11. Recent biochemical data from *S. cerevisiae* and *S. pombe* implicate Mre11 as the nuclease that removes the covalently bound Spo11 from meiotic DSBs (Neale *et al.* 2005). On the basis of their predicted structures (Figures 1C and 2), we expect that Rad50-8 and Rad50-14 retain the ability to interact with Mre11. Although Rad50-15 is missing the N-terminal portion of the Mre11 binding site, its phenotype predicts that Rad50-15 does interact with Mre11 as well.

Although our data show that catalytic activity by the Rad50 molecules themselves cannot be essential for AE formation or meiotic DSB processing, none of the Rad50 mutant proteins allows the formation of wild-type levels of SC, and all mutant strains arrest in meiosis.

Therefore, enzymatic activity conferred by intact C- and N-terminal globular domains is necessary for complete synapsis and meiotic progression.

What is the role of Rad50 in AE formation? AE formation results from structural changes in meiotic chromatin that may require Rad50 or require Rad50 for stability. In comparison to wild-type *S. cerevisiae* meiotic cells, *rad50*Δ strains show increased sensitivity of DNA to micrococcal nuclease treatment (Ohta *et al.* 1998). It is possible that in the absence of Rad50, or of its coiled-coil regions, structural changes of the chromatin do not occur, and AE cannot form. It is additionally possible that Rad50 has a structural role either in the AE core itself or in mediating appropriate sister-chromatid interactions that are necessary for AE formation. In *S. pombe rad50*Δ mutants, sister-chromatid recombination is reduced and homologous recombination frequencies are increased (Hartsuiker *et al.* 2001). The same is true of homologous recombination frequencies in *S. cerevisiae rad50*Δ strains (Malone *et al.* 1990). Haploid *rad50*Δ G_2 strains are more sensitive to radiation than diploid *rad50*Δ G_1 strains, suggesting that Rad50 is associated with sister-chromatid interactions (Fabre *et al.* 1984; Ivanov *et al.* 1992; Paques and Haber 1999). Additionally, a *C. cinereus rad50-4;msh5-22* double mutant, which enters meiosis with unreplicated chromosomes, is rescued for SC formation (Merino *et al.* 2000). Therefore, the role of Rad50 in AE formation could also be due to its requirement in sister-chromatid interactions. Although a recent study found no loss of mitotic sister-chromatid cohesion in *rad50* mutants of *S. cerevisiae* (Wiltzius *et al.* 2005), there are several lines of study that argue that meiotic recombination imposes additional requirements for sister-chromatid cohesion. First, DSB repair requires the recruitment of additional cohesin to sites of DNA damage (Strom *et al.* 2004; Unal *et al.* 2004). Cohesin recruitment to DSB sites requires Mre11, and although it is unknown whether the entire MRN complex is necessary, Mre11 does not localize to chromatin in the absence of Nbs1 (Tauchi *et al.* 2001), arguing that complex formation is necessary. Second, a *spo11* mutation partially suppresses the need for Rec8 and Spo76 in *Sordaria macrospora* (Storlazzi *et al.* 2008), meaning that chiasma formation imposes an increased requirement for cohesion. Finally, the *rad9-1* mutant of *C. cinereus* has no obvious mitotic growth defect but is almost completely defective in meiosis (Zolan *et al.* 1988). Rad9 is the *C. cinereus* ortholog of *S. cerevisiae* Scc2 (Michaelis *et al.* 1997), *S. pombe* Mis4 (Furuya *et al.* 1998), *D. melanogaster* NippedB (Rollins *et al.* 1999), and the human delangin protein (Krantz *et al.* 2004; Tonkin *et al.* 2004) and is required for cohesin localization to chromatin (Ciosk *et al.* 2000). The difference in mitotic and meiotic phenotypes for *rad9-1* argues for an enhanced role of sister-chromatid cohesion in meiosis. Because Rad50 is an SMC-like protein, structurally similar to members of condensin and cohesin complexes (Losada and Hirano 2005; Nasmyth and Haering 2005), its role in meiotic sister-chromatid interactions may be as a member of the MRN complex, required for cohesin recruitment (Strom *et al.* 2004; Unal *et al.* 2004), or the Rad50 protein may be structurally required for appropriate sister-chromatid interactions. These two roles are not mutually exclusive, and it is also possible that the modification of chromatin structure by Rad50 may be a key factor in cohesin recruitment to sites of recombination.

We thank Claire Walczak and Joel Ybe for assistance in developing antibody purification techniques, Ellen Quardokus for immunofluorescence assistance and advice, and Jim Bever for statistics advice. We also thank F. Rudolph Turner for preparation of electron micrographs, Katy Van Hook for preliminary antibody purification work, Martha Oakley for helpful discussion, Pat Pukkila and Elizabeth A. Sierra for helpful discussion and critical reading of the manuscript, and Megan Kingslover for clerical support. In addition, we thank Kengo Sakaguchi and his laboratory for their generous gift of the Dmc1 expression construct. This work was supported by National Institutes of Health grants GM43930 (to M.E.Z.), CA117638 and CA092584 (to J.A.T.), and (training grant) T32 GMOO7757 (to S.N.A.).

LITERATURE CITED

Ajimura, M., S. H. Leem and H. Ogawa, 1993 Identification of new genes required for meiotic recombination in *Saccharomyces cerevisiae*. Genetics **133:** 51–66.

Alani, E., R. Padmore and N. Kleckner, 1990 Analysis of wild-type and rad50 mutants of yeast suggests an intimate relationship between meiotic chromosome synapsis and recombination. Cell **61:** 419–436.

Altschul, S. F., W. Gish, W. Miller, E. W. Myers and D. J. Lipman, 1990 Basic local alignment search tool. J. Mol. Biol. **215:** 403–410.

Altschul, S. F., T. L. Madden, A. A. Schaffer, J. Zhang, Z. Zhang *et al.*, 1997 Gapped BLAST and PSI-BLAST: a new generation of protein database search programs. Nucleic Acids Res. **25:** 3389–3402.

Bender, C. F., M. L. Sikes, R. Sullivan, L. E. Huye, M. M. Le Beau *et al.*, 2002 Cancer predisposition and hematopoietic failure in Rad50(S/S) mice. Genes Dev. **16:** 2237–2251.

Bhaskara, V., A. Dupre, B. Lengsfeld, B. B. Hopkins, A. Chan *et al.*, 2007 Rad50 adenylate kinase activity regulates DNA tethering by Mre11/Rad50 complexes. Mol. Cell **25:** 647–661.

Binninger, D. M., C. Skrzynia, P. J. Pukkila and L. A. Casselton, 1987 DNA-mediated transformation of the basidiomycete Coprinus cinereus. EMBO J. **6:** 835–840.

Borde, V., 2007 The multiple roles of the Mre11 complex for meiotic recombination. Chromosome Res. **15:** 551–563.

Cao, L., E. Alani and N. Kleckner, 1990 A pathway for generation and processing of double-strand breaks during meiotic recombination in S. cerevisiae. Cell **61:** 1089–1101.

Carney, J. P., R. S. Maser, H. Olivares, E. M. Davis, M. Le Beau *et al.*, 1998 The hMre11/hRad50 protein complex and Nijmegen breakage syndrome: linkage of double-strand break repair to the cellular DNA damage response. Cell **93:** 477–486.

Celerin, M., S. T. Merino, J. E. Stone, A. M. Menzie and M. E. Zolan, 2000 Multiple roles of Spo11 in meiotic chromosome behavior. EMBO J. **19:** 2739–2750.

Cha, R. S., B. M. Weiner, S. Keeney, J. Dekker and N. Kleckner, 2000 Progression of meiotic DNA replication is modulated by interchromosomal interaction proteins, negatively by Spo11p and positively by Rec8p. Genes Dev. **14:** 493–503.

Chamankhah, M., Y. F. Wei and W. Xiao, 1998 Isolation of hMRE11B: failure to complement yeast mre11 defects due to species-specific protein interactions. Gene **225:** 107–116.

Cherry, S. M., C. A. Adelman, J. W. Theunissen, T. J. Hassold, P. A. Hunt *et al.*, 2007 The Mre11 complex influences DNA repair, synapsis, and crossing over in murine meiosis. Curr. Biol. **17:** 373–378.

Ciosk, R., M. Shirayama, A. Shevchenko, T. Tanaka, A. Toth *et al.*, 2000 Cohesin's binding to chromosomes depends on a separate complex consisting of Scc2 and Scc4 proteins. Mol. Cell **5:** 243–254.

Cox, B. S., and J. M. Parry, 1968 The isolation, genetics and survival characteristics of ultraviolet light-sensitive mutants in yeast. Mutat. Res. **6:** 37–55.

Cummings, W. J., M. Celerin, J. Crodian, L. K. Brunick and M. E. Zolan, 1999 Insertional mutagenesis in Coprinus cinereus: use of a dominant selectable marker to generate tagged, sporulation-defective mutants. Curr. Genet. **36:** 371–382.

Cummings, W. J., S. T. Merino, K. G. Young, L. Li, C. W. Johnson *et al.*, 2002 The Coprinus cinereus adherin Rad9 functions in Mre11-dependent DNA repair, meiotic sister-chromatid cohesion, and meiotic homolog pairing. Proc. Natl. Acad. Sci. USA **99:** 14958–14963.

de Jager, M., K. M. Trujillo, P. Sung, K. P. Hopfner, J. P. Carney *et al.*, 2004 Differential arrangements of conserved building blocks among homologs of the Rad50/Mre11 DNA repair protein complex. J. Mol. Biol. **339:** 937–949.

Dolganov, G. M., R. S. Maser, A. Novikov, L. Tosto, S. Chong *et al.*, 1996 Human Rad50 is physically associated with human Mre11: identification of a conserved multiprotein complex implicated in recombinational DNA repair. Mol. Cell. Biol. **16:** 4832–4841.

Fabre, F., A. Boulet and H. Roman, 1984 Gene conversion at different points in the mitotic cycle of Saccharomyces cerevisiae. Mol. Gen. Genet. **195:** 139–143.

Furuya, K., K. Takahashi and M. Yanagida, 1998 Faithful anaphase is ensured by Mis4, a sister chromatid cohesion molecule required in S phase and not destroyed in G1 phase. Genes Dev. **12:** 3408–3418.

Gallego, M. E., M. Jeanneau, F. Granier, D. Bouchez, N. Bechtold *et al.*, 2001 Disruption of the Arabidopsis RAD50 gene leads to plant sterility and MMS sensitivity. Plant J. **25:** 31–41.

Game, J. C., T. J. Zamb, R. J. Braun, M. Resnick and R. M. Roth, 1980 The role of radiation (rad) genes in meiotic recombination in yeast. Genetics **94:** 51–68.

Gasior, S. L., A. K. Wong, Y. Kora, A. Shinohara and D. K. Bishop, 1998 Rad52 associates with RPA and functions with rad55 and rad57 to assemble meiotic recombination complexes. Genes Dev. **12:** 2208–2221.

Gerecke, E. E., and M. E. Zolan, 2000 An mre11 mutant of Coprinus cinereus has defects in meiotic chromosome pairing, condensation and synapsis. Genetics **154:** 1125–1139.

Hartsuiker, E., E. Vaessen, A. M. Carr and J. Kohli, 2001 Fission yeast Rad50 stimulates sister chromatid recombination and links cohesion with repair. EMBO J. **20:** 6660–6671.

Hayashi, M., G. M. Chin and A. M. Villeneuve, 2007 C. elegans germ cells switch between distinct modes of double-strand break repair during meiotic prophase progression. PLoS Genet. **3:** e191.

Herskowitz, I., 1987 Functional inactivation of genes by dominant negative mutations. Nature **329:** 219–222.

Holzen, T. M., P. P. Shah, H. A. Olivares and D. K. Bishop, 2006 Tid1/Rdh54 promotes dissociation of Dmc1 from nonrecombinogenic sites on meiotic chromatin. Genes Dev. **20:** 2593–2604.

Hopfner, K. P., and J. A. Tainer, 2003 Rad50/SMC proteins and ABC transporters: unifying concepts from high-resolution structures. Curr. Opin. Struct. Biol. **13:** 249–255.

Hopfner, K. P., A. Karcher, D. Shin, C. Fairley, J. A. Tainer *et al.*, 2000a Mre11 and Rad50 from Pyrococcus furiosus: cloning and biochemical characterization reveal an evolutionarily conserved multiprotein machine. J. Bacteriol. **182:** 6036–6041.

Hopfner, K. P., A. Karcher, D. S. Shin, L. Craig, L. M. Arthur *et al.*, 2000b Structural biology of Rad50 ATPase: ATP-driven conformational control in DNA double-strand break repair and the ABC-ATPase superfamily. Cell **101:** 789–800.

Hopfner, K. P., A. Karcher, L. Craig, T. T. Woo, J. P. Carney *et al.*, 2001 Structural biochemistry and interaction architecture of the DNA double-strand break repair Mre11 nuclease and Rad50-ATPase. Cell **105:** 473–485.

Hopfner, K. P., L. Craig, G. Moncalian, R. A. Zinkel, T. Usui *et al.*, 2002a The Rad50 zinc-hook is a structure joining Mre11 complexes in DNA recombination and repair. Nature **418:** 562–566.

Hopfner, K. P., C. D. Putnam and J. A. Tainer, 2002b DNA double-strand break repair from head to tail. Curr. Opin. Struct. Biol. **12:** 115–122.

Ivanov, E. L., V. G. Korolev and F. Fabre, 1992 XRS2, a DNA repair gene of *Saccharomyces cerevisiae*, is needed for meiotic recombination. Genetics **132:** 651–664.

Johzuka, K., and H. Ogawa, 1995 Interaction of Mre11 and Rad50: two proteins required for DNA repair and meiosis-specific double-strand break formation in Saccharomyces cerevisiae. Genetics **139:** 1521–1532.

Keeney, S., 2008 Spo11 and the formation of DNA double-strand breaks in meiosis, pp. 81–123 in *Recombination and Meiosis*, edited by R. Egel and D.-H. Lankenau. Springer, Berlin/Heidelberg, Germany.

Keeney, S., C. N. Giroux and N. Kleckner, 1997 Meiosis-specific DNA double-strand breaks are catalyzed by Spo11, a member of a widely conserved protein family. Cell **88:** 375–384.

Kleckner, N., 2006 Chiasma formation: chromatin/axis interplay and the role(s) of the synaptonemal complex. Chromosoma **115:** 175–194.

Krantz, I. D., J. McCallum, C. DeScipio, M. Kaur, L. A. Gillis *et al.*, 2004 Cornelia de Lange syndrome is caused by mutations in NIPBL, the human homolog of Drosophila melanogaster Nipped-B. Nat. Genet. **36:** 631–635.

Kraulis, P. J., 1991 Molscript—a program to produce both detailed and schematic plots of protein structures. J. Appl. Crystallogr. **24:** 946–950.

Lee, J. H., and T. T. Paull, 2004 Direct activation of the ATM protein kinase by the Mre11/Rad50/Nbs1 complex. Science **304:** 93–96.

Lee, J. H., and T. T. Paull, 2005 ATM activation by DNA double-strand breaks through the Mre11-Rad50-Nbs1 complex. Science **308:** 551–554.

Li, L., E. E. Gerecke and M. E. Zolan, 1999 Homolog pairing and meiotic progression in Coprinus cinereus. Chromosoma **108:** 384–392.

Losada, A., and T. Hirano, 2005 Dynamic molecular linkers of the genome: the first decade of SMC proteins. Genes Dev. **19:** 1269–1287.

Luo, G., M. S. Yao, C. F. Bender, M. Mills, A. R. Bladl *et al.*, 1999 Disruption of mRad50 causes embryonic stem cell lethality, abnormal embryonic development, and sensitivity to ionizing radiation. Proc. Natl. Acad. Sci. USA **96:** 7376–7381.

Malone, R. E., 1983 Multiple mutant analysis of recombination in yeast. Mol. Gen. Genet. **189:** 405–412.

Malone, R. E., and R. E. Esposito, 1981 Recombinationless meiosis in Saccharomyces cerevisiae. Mol. Cell. Biol. **1:** 891–901.

Malone, R. E., T. Ward, S. Lin and J. Waring, 1990 The RAD50 gene, a member of the double strand break repair epistasis group, is not required for spontaneous mitotic recombination in yeast. Curr. Genet. **18:** 111–116.

Matsuura, S., H. Tauchi, A. Nakamura, N. Kondo, S. Sakamoto *et al.*, 1998 Positional cloning of the gene for Nijmegen breakage syndrome. Nat. Genet. **19:** 179–181.

Mehrotra, S., and K. S. McKim, 2006 Temporal analysis of meiotic DNA double-strand break formation and repair in Drosophila females. PLoS Genet. **2:** e200.

Merino, S. T., W. J. Cummings, S. N. Acharya and M. E. Zolan, 2000 Replication-dependent early meiotic requirement for Spo11 and Rad50. Proc. Natl. Acad. Sci. USA **97:** 10477–10482.

Michaelis, C., R. Ciosk and K. Nasmyth, 1997 Cohesins: chromosomal proteins that prevent premature separation of sister chromatids. Cell **91:** 35–45.

Moncalian, G., B. Lengsfeld, V. Bhaskara, K. P. Hopfner, A. Karcher *et al.*, 2004 The rad50 signature motif: essential to ATP binding and biological function. J. Mol. Biol. **335:** 937–951.

Moreno-Herrero, F., M. de Jager, N. H. Dekker, R. Kanaar, C. Wyman *et al.*, 2005 Mesoscale conformational changes in the DNA-repair complex Rad50/Mre11/Nbs1 upon binding DNA. Nature **437:** 440–443.

Nairz, K., and F. Klein, 1997 mre11S–a yeast mutation that blocks double-strand-break processing and permits nonhomologous synapsis in meiosis. Genes Dev. **11:** 2272–2290.

Nara, T., F. Hamada, S. Namekawa and K. Sakaguchi, 2001 Strand exchange reaction in vitro and DNA-dependent ATPase activity

of recombinant LIM15/DMC1 and RAD51 proteins from Coprinus cinereus. Biochem. Biophys. Res. Commun. **285:** 92–97.

Nasmyth, K., and C. H. Haering, 2005 The structure and function of SMC and kleisin complexes. Annu. Rev. Biochem. **74:** 595–648.

Neale, M. J., J. Pan and S. Keeney, 2005 Endonucleolytic processing of covalent protein-linked DNA double-strand breaks. Nature **436:** 1053–1057.

Ohta, K., A. Nicolas, M. Furuse, A. Nabetani, H. Ogawa *et al.*, 1998 Mutations in the MRE11, RAD50, XRS2, and MRE2 genes alter chromatin configuration at meiotic DNA double-stranded break sites in premeiotic and meiotic cells. Proc. Natl. Acad. Sci. USA **95:** 646–651.

Paques, F., and J. E. Haber, 1999 Multiple pathways of recombination induced by double-strand breaks in Saccharomyces cerevisiae. Microbiol. Mol. Biol. Rev. **63:** 349–404.

Pauli, T. T., and M. Gellert, 1998 The 3′ to 5′ exonuclease activity of Mre 11 facilitates repair of DNA double-strand breaks. Mol. Cell **1:** 969–979.

Pauli, T. T., and M. Gellert, 1999 Nbs1 potentiates ATP-driven DNA unwinding and endonuclease cleavage by the Mre11/Rad50 complex. Genes Dev. **13:** 1276–1288.

Petrini, J. H., M. E. Walsh, C. DiMare, X. N. Chen, J. R. Korenberg *et al.*, 1995 Isolation and characterization of the human MRE11 homologue. Genomics **29:** 80–86.

Pitts, S. A., H. S. Kullar, T. Stankovic, G. S. Stewart, J. I. Last *et al.*, 2001 hMRE11: genomic structure and a null mutation identified in a transcript protected from nonsense-mediated mRNA decay. Hum. Mol. Genet. **10:** 1155–1162.

Puizina, J., J. Siroky, P. Mokros, D. Schweizer and K. Riha, 2004 Mre11 deficiency in Arabidopsis is associated with chromosomal instability in somatic cells and Spo11-dependent genome fragmentation during meiosis. Plant Cell **16:** 1968–1978.

Pukkila, P. J., and B. C. Lu, 1985 Silver staining of meiotic chromosomes in the fungus, Coprinus cinereus. Chromosoma **91:** 108–112.

Pukkila, P. J., B. M. Yashar and D. M. Binninger, 1984 Analysis of meiotic development in Coprinus cinereus, pp. 177–194 in *Controlling Events in Meiosis*, edited by C. W. Evans and H. G. Dickinson. Society for Experimental Biology, Cambridge, UK.

Pukkila, P. J., C. Skrzynia and B. C. Lu, 1992 The *rad3-1* mutant is defective in axial core assembly and homologous chromosome pairing during meiosis in the basidiomycete *Coprinus cinereus*. Dev. Genet. **13:** 403–410.

Raju, N. B., and B. C. Lu, 1970 Meiosis in Coprinus. III. Timing of meiotic events in C. lagopus (sensu Buller). Can. J. Bot. **48:** 2183–2186.

Ramesh, M. A., and M. E. Zolan, 1995 Chromosome dynamics in rad12 mutants of Coprinus cinereus. Chromosoma **104:** 189–202.

Raymond, W. E., and N. Kleckner, 1993 RAD50 protein of S. cerevisiae exhibits ATP-dependent DNA binding. Nucleic Acids Res. **21:** 3851–3856.

Rollins, R. A., P. Morcillo and D. Dorsett, 1999 Nipped-B, a Drosophila homologue of chromosomal adherins, participates in activation by remote enhancers in the cut and Ultrabithorax genes. Genetics **152:** 577–593.

Seitz, L. C., K. Tang, W. J. Cummings and M. E. Zolan, 1996 The rad9 gene of Coprinus cinereus encodes a proline-rich protein required for meiotic chromosome condensation and synapsis. Genetics **142:** 1105–1117.

Sharples, G. J., and D. R. Leach, 1995 Structural and functional similarities between the SbcCD proteins of Escherichia coli and the RAD50 and MRE11 (RAD32) recombination and repair proteins of yeast. Mol. Microbiol. **17:** 1215–1217.

Stajich, J. E., B. Birren, C. Burns, L. A. Casselton, F. Dietrich *et al.*, 2006 Genomic analysis of *Coprinus cinereus*. Proceedings of the International Symposium on Mushroom Science, pp. 59–66. Akita Prefectural University, Akita, Japan.

Stassen, N. Y., J. M. Logsdon, Jr., G. J. Vora, H. H. Offenberg, J. D. Palmer *et al.*, 1997 Isolation and characterization of rad51 orthologs from Coprinus cinereus and Lycopersicon esculentum, and phylogenetic analysis of eukaryotic recA homologs. Curr. Genet. **31:** 144–157.

Stewart, G. S., R. S. Maser, T. Stankovic, D. A. Bressan, M. I. Kaplan *et al.*, 1999 The DNA double-strand break repair gene hMRE11 is mutated in individuals with an ataxia-telangiectasia-like disorder. Cell **99:** 577–587.

Storlazzi, A., S. Tesse, G. Ruprich-Robert, S. Gargano, S. Poggeler *et al.*, 2008 Coupling meiotic chromosome axis integrity to recombination. Genes Dev. **22:** 796–809.

Strom, L., H. B. Lindroos, K. Shirahige and C. Sjogren, 2004 Postreplicative recruitment of cohesin to double-strand breaks is required for DNA repair. Mol. Cell **16:** 1003–1015.

Sym, M., J. A. Engebrecht and G. S. Roeder, 1993 ZIP1 is a synaptonemal complex protein required for meiotic chromosome synapsis. Cell **72:** 365–378.

Tauchi, H., J. Kobayashi, K. Morishima, S. Matsuura, A. Nakamura *et al.*, 2001 The forkhead-associated domain of NBS1 is essential for nuclear foci formation after irradiation but not essential for hRAD50·hMRE11·NBS1 complex DNA repair activity. J. Biol. Chem. **276:** 12–15.

Tavassoli, M., M. Shayeghi, A. Nasim and F. Z. Watts, 1995 Cloning and characterisation of the Schizosaccharomyces pombe rad32 gene: a gene required for repair of double strand breaks and recombination. Nucleic Acids Res. **23:** 383–388.

Thompson, J. D., T. J. Gibson, F. Plewniak, F. Jeanmougin and D. G. Higgins, 1997 The CLUSTAL_X windows interface: flexible strategies for multiple sequence alignment aided by quality analysis tools. Nucleic Acids Res. **25:** 4876–4882.

Tonkin, E. T., T. J. Wang, S. Lisgo, M. J. Bamshad and T. Strachan, 2004 NIPBL, encoding a homolog of fungal Scc2-type sister chromatid cohesion proteins and fly Nipped-B, is mutated in Cornelia de Lange syndrome. Nat. Genet. **36:** 636–641.

Trujillo, K. M., S. S. Yuan, E. Y. Lee and P. Sung, 1998 Nuclease activities in a complex of human recombination and DNA repair factors Rad50, Mre11, and p95. J. Biol. Chem. **273:** 21447–21450.

Unal, E., A. Arbel-Eden, U. Sattler, R. Shroff, M. Lichten *et al.*, 2004 DNA damage response pathway uses histone modification to assemble a double-strand break-specific cohesin domain. Mol. Cell **16:** 991–1002.

Valentine, G., Y. J. Wallace, F. R. Turner and M. E. Zolan, 1995 Pathway analysis of radiation-sensitive meiotic mutants of Coprinus cinereus. Mol. Gen. Genet. **247:** 169–179.

Varon, R., C. Vissinga, M. Platzer, K. M. Cerosaletti, K. H. Chrzanowska *et al.*, 1998 Nibrin, a novel DNA double-strand break repair protein, is mutated in Nijmegen breakage syndrome. Cell **93:** 467–476.

Williams, R. S., and J. A. Tainer, 2005 A nanomachine for making ends meet: MRN is a flexing scaffold for the repair of DNA double-strand breaks. Mol. Cell **19:** 724–726.

Williams, R. S., J. S. Williams and J. A. Tainer, 2007 Mre11-Rad50-Nbs1 is a keystone complex connecting DNA repair machinery, double-strand break signaling, and the chromatin template. Biochem. Cell Biol. **85:** 509–520.

Williams, R. S., G. Moncalian, J. S. Williams, Y. Yamada, O. Limbo *et al.*, 2008 Mre11 dimers coordinate DNA end bridging and nuclease processing in double strand break repair. Cell **135:** 97–109.

Wiltzius, J., M. Hohl, J. Fleming and J. Petrini, 2005 The Rad50 hook domain is a critical determinant of Mre11 complex functions. Nat. Struct. Mol. Biol. **12:** 403–407.

Wolf, E., P. S. Kim and B. Berger, 1997 MultiCoil: a program for predicting two- and three-stranded coiled coils. Protein Sci. **6:** 1179–1189.

Wu, M. M. J., J. R. Cassidy and P. J. Pukkila, 1983 Polymorphisms in DNA of *Coprinus cinereus*. Curr. Genet. **7:** 385–392.

Xiao, Y., and D. T. Weaver, 1997 Conditional gene targeted deletion by Cre recombinase demonstrates the requirement for the double-strand break repair Mre11 protein in murine embryonic stem cells. Nucleic Acids Res. **25:** 2985–2991.

Yamaguchi-Iwai, Y., E. Sonoda, M. S. Sasaki, C. Morrison, T. Haraguchi *et al.*, 1999 Mre11 is essential for the maintenance of chromosomal DNA in vertebrate cells. EMBO J. **18:** 6619–6629.

Young, J. A., R. W. Hyppa and G. R. Smith, 2004 Conserved and nonconserved proteins for meiotic DNA breakage and repair in yeasts. Genetics **167:** 593–605.

Zhu, J., S. Petersen, L. Tessarollo and A. Nussenzweig, 2001 Targeted disruption of the Nijmegen breakage syndrome gene NBS1 leads to early embryonic lethality in mice. Curr. Biol. **11:** 105–109.

Zolan, M. E., and P. J. Pukkila, 1986 Inheritance of DNA methylation in Coprinus cinereus. Mol. Cell. Biol. **6:** 195–200.

Zolan, M. E., C. J. Tremel and P. J. Pukkila, 1988 Production and characterization of radiation-sensitive meiotic mutants of *Coprinus cinereus*. Genetics **120:** 379–387.

Zolan, M. E., J. R. Crittenden, N. K. Heyler and L. C. Seitz, 1992 Efficient isolation and mapping of rad genes of the fungus Coprinus cinereus using chromosome-specific libraries. Nucleic Acids Res. **20:** 3993–3999.

Zolan, M. E., N. K. Heyler and M. A. Ramesh, 1993 Gene mapping using marker chromosomes in Coprinus cinereus, pp. 31–35 in *Industrial Microorganisms: Basic and Applied Molecular Genetics*, edited by R. H. Baltz, G. D. Hegeman and P. L. Skatrud. American Society for Microbiology, Washington, DC.

Zolan, M. E., N. Yeager, Y. Stassen, M. A. Ramesh, B. C. Lu *et al.*, 1995 Meiotic mutants and DNA repair genes of *Coprinus cinereus*. Can. J. Bot. Rev. Can. Bot. **73:** S226–S233.

Communicating editor: G. P. Copenhaver